◆ Human Brain Mapping 35:5754–5775 (2014) ◆

Isoflurane Induces Dose-Dependent Alterations in the Cortical Connectivity Profiles and Dynamic Properties of the Brain's Functional Architecture

R. Matthew Hutchison,[1,2,3]* Melina Hutchison,[4] Kathryn Y. Manning,[1] Ravi S. Menon,[1] and Stefan Everling[1,5]

[1]*Robarts Research Institute, University of Western Ontario, London, Ontario, Canada*
[2]*Department of Psychology, Harvard University, Cambridge, Massachusetts*
[3]*Center for Brain Science, Harvard University, Cambridge, Massachusetts*
[4]*London Health Sciences Centre, London, Ontario, Canada*
[5]*Department of Physiology and Pharmacology, University of Western Ontario, London Ontario, Canada*

Abstract: Despite their widespread use, the effect of anesthetic agents on the brain's functional architecture remains poorly understood. This is particularly true of alterations that occur beyond the point of induced unconsciousness. Here, we examined the distributed intrinsic connectivity of macaques across six isoflurane levels using resting-state functional MRI (fMRI) following the loss of consciousness. The results from multiple analysis strategies showed stable functional connectivity (FC) patterns between 1.00% and 1.50% suggesting this as a suitable range for anesthetized nonhuman primate resting-state investigations. Dose-dependent effects were evident at moderate to high dosages showing substantial alteration of the functional topology and a decrease or complete loss of interhemispheric cortical FC strength including that of contralateral homologues. The assessment of dynamic FC patterns revealed that the functional repertoire of brain states is related to anesthesia depth and most strikingly, that the number of state transitions linearly decreases with increased isoflurane dosage. Taken together, the results indicate dose-specific spatial and temporal alterations of FC that occur beyond the typically defined endpoint of consciousness. Future work will be necessary to determine how these findings generalize across anesthetic types and extend to the transition between consciousness and unconsciousness. *Hum Brain Mapp 35:5754–5775, 2014.*

Key words: anesthesia; consciousness; connectivity; functional repertoire resting-state functional MRI

Additional Supporting Information may be found in the online version of this article.

Contract grant sponsor: Canadian Institutes of Health Research (CIHR); Contract grant numbers: MOP-89785 (S.E.); PRG-165679 (R.S.M.); postdoctoral fellowship (R.M.H.)

*Correspondence to: R. Matthew Hutchison, Center for Brain Science, Harvard University, Northwest Building- East Wing, 52 Oxford Street, Cambridge, MA 02138, E-mail: rhutchison@FAS.harvard.edu

Received for publication 30 December 2013; Revised 5 June 2014; Accepted 2 July 2014.

DOI: 10.1002/hbm.22583

Published online 12 July 2014 in Wiley Online Library (wileyonlinelibrary.com).

INTRODUCTION

General anesthetics allow for a pharmacologically induced and reversible alteration of consciousness that is accompanied by various degrees of amnesia, analgesia, immobility, and attenuation of autonomic responses. However, their routine use during surgical procedures obscures the fact that the precise mechanism of action of most anesthetic agents remains poorly understood. There is substantial motivation from clinicians to elucidate the fundamental features of anesthesia, as the results can have significant impact on the delivery and development of the agents, and also for neuroscientists, who exploit anesthetics to investigate the emergence and breakdown of brain states in a controlled manner. The majority of studies examining the effects of anesthesia on consciousness have been conducted at the level of receptors and single unit activity. While the various anesthetics differently affect ion channels (to varying degrees and direction of potentiation), making a single mechanism of anesthetic action in unconsciousness elusive, many theories attempt to resolve these discrepancies by extrapolating the local effects to a more large-scale or global level [Alkire et al., 2008; Brown et al., 2011; Franks, 2006].

The information integration theory of consciousness suggests that the capacity of a system to integrate information across local and remote brain areas is the quintessential element of consciousness [Tononi, 2004]. The loss of consciousness during anesthesia could then be associated with a disruption of integration seen as a breakdown of either large-scale communication between brain regions or information content as reflected in the repertoire of activity patterns [Alkire et al., 2008]. The theory also posits that consciousness is not an all-or-none phenomenon, but graded, decreasing proportionately with the number of discriminable states that may collapse nonlinearly [Tononi, 2004]. This could suggest that functional integration and state expression may continue to break down beyond the typical endpoint of unconsciousness. Therefore, the study of different levels of anesthesia may provide valuable insight into functional brain architecture, consciousness, and mechanisms of anesthesia.

Resting-state functional MRI (RS-fMRI) is particularly well-suited to explore anesthesia-related changes as it allows for the noninvasive assessment of whole brain functional interactions in the absence of any explicit task. The spontaneous, low-frequency (~0.01–0.1 Hz) blood oxygenation level-dependent (BOLD) signals recorded with the technique have been shown to reflect (at least partially) the underlying neuronal activity [Shmuel and Leopold, 2008; for reviews, see Fox and Raichle 2007, Leopold and Maier 2012 and importantly, evaluation of their temporal dependencies have revealed robust and reliable connectivity maps [e.g., Biswal et al., 1995; Beckmann et al., 2005; Damoiseaux et al., 2006; for review, see Fox and Raichle, 2007] across multiple species [e.g., Hutchison et al., 2010, 2011; Kannurpatti et al., 2008; Liang et al., 2011; Pawela et al., 2008; Vincent et al., 2007; for review see Hutchison and Everling, 2012]. The technique can serve to extend positron emission tomography (PET) investigations that have provided critical findings related to anesthesia's metabolic effects [e.g., Alkire et al., 1997, 1999]. RS-fMRI examination of anesthesia effects has been primarily concerned with functional connectivity (FC) changes related to awake versus unconscious (or sedated) states [Boveroux et al., 2010; Deshpande et al., 2010; Greicius et al., 2008; Kiviniemi et al., 2000, 2005; Liang et al., 2012; Liu et al., 2011, 2013b; Moeller et al., 2009; Peltier et al., 2005], anesthetic type [Hutchison et al., 2010; Kalthoff et al., 2013], or dose-dependencies [Deshpande et al., 2010; Liu et al., 2011, 2013b; Lu et al., 2007; Peltier et al., 2005; Vincent et al., 2007; Wang et al., 2011] using a variety of anesthetics in several mammalian species [for reviews, see Bonhomme et al., 2012; Heine et al., 2012; Hudetz, 2012; Nallasamy and Tsao, 2011]. The studies have reported mixed results that indicate both increases and decreases in functional integration within select (typically higher order) intrinsic connectivity networks (ICNs) that correlated with anesthesia-induced unconsciousness. While the reasons for the inconsistencies, possibly related to drug type and dosage—both of which have shown to differentially affect connectivity patterns—need to be determined, the findings point toward altered functional integration as a mechanism of unconsciousness.

Overall, relatively little is known about the large-scale, dose-dependent nature of anesthetic changes in spontaneous functional interactions, particularly after unconsciousness has been induced. The previous RS-fMRI studies that have investigated increasing anesthetic levels often characterize dosages in broad terms (e.g., light vs. deep) that may obscure more fine-grained differences, and in many cases, only consider the activity within selected networks that prevents characterization of the brain's overall functional architecture [Deshpande et al., 2010; Liu et al., 2011, 2012; Lu et al., 2007; Peltier et al., 2005; Vincent et al., 2007; Wang et al., 2011]. Recent work is now beginning to highlight the graded effects that can occur as anesthetic agents are systematically varied [Liu et al., 2013a, b]. Further, the conclusions are based solely on static characterizations of FC, not taking into account possible dynamic FC changes that could reveal level-dependent repertoire changes [for review, see Hutchison et al., 2013a].

Here, we investigated the dose-dependent effects of isoflurane, a halogenated ether that has diffuse and divergent molecular effects, on the FC patterns in the nonhuman primate following induction of unconsciousness. The use of this animal model circumvents concerns of potentially inducing a lethal collapse of the cardiovascular or respiratory system at higher dosages in humans as well as offering greater standardization between subjects. We had two primary objectives. The first was to determine if increasing isoflurane doses across levels following the loss of consciousness resulted in graded changes in large-scale network architecture as assessed using RS-fMRI. At this

spatial level, two different mechanisms concerning the loss of information integration have been proposed [Alkire et al., 2008; Hudetz, 2006]. The first suggests that at suprathreshold levels of anesthesia, FC will nonuniformly break down and result in decreased correlation patterns [Deshpande et al., 2010; Lu et al., 2007; Peltier et al., 2005], while the other proposes a global loss of functional segregation that should manifest as a substantial reduction in the specificity of connectivity patterns [Kalthoff et al., 2013; Liu et al., 2011, 2013b]. The second objective was to determine if the functional repertoire and dynamic reconfigurations of spontaneous brain states occurring in unconscious animals vary as a function of the anesthetic depth. It has been suggested that during deep anesthesia, the variability in large-scale neural patterns shrinks (equating to a loss of information), eventually leading to a stereotypic burst-suppression pattern with only two possible states [on or off; Alkire et al., 2008]. We tested this by examining whole-brain FC states across anesthesia levels using a dynamic RS-fMRI approach.

METHODS

Animal Preparation

All surgical and experimental procedures were carried out in accordance with the Canadian Council of Animal Care policy on the use of laboratory animals and approved by the Animal Use Subcommittee of the University of Western Ontario Council on Animal Care. Data were collected from five macaque monkeys (*Macaca fascicularis*; four females) whose weights ranged from 3.6 to 5.3 kg (mean ± standard deviation = 4.26 ± 0.76 kg) and ages ranged from 7.71 to 8.22 years (mean ± standard deviation = 7.83 ± 0.22 years). All animals were previously (>3 years) implanted with an MRI-compatible custom-built acrylic head post that was anchored to the skull with 6-mm ceramic bone screws (Thomas Recording, Giessen, Germany) and dental acrylic to allow restraint of the head during data collection.

In preparation for image acquisition, monkeys were injected intramuscularly with atropine (0.4 mg/kg), ipratropium (0.025 mg/kg), and ketamine hydrochloride (7.5 mg/kg), followed by intravenous administration of 3 ml propofol (10 mg/ml) via the saphenous vein. Animals were then intubated and switched to 1.5% isoflurane mixed with medical air. Each monkey was then placed in a custom-built monkey chair with its head immobilized using the head post, and inserted into the magnet bore, at which time the isoflurane level was lowered to 1.00%. At least 30 min was allowed for the isoflurane level and global hemodynamics to stabilize at the 1.00% concentration, during which the image localization, shimming, and test echo-planar imaging (EPI) were performed. Two scans at six increasing isoflurane levels at 1.00, 1.25, 1.50, 1.75, 2.00, and 2.75% (0.78, 0.98, 1.17, 1.37, 1.56, and 2.15 minimum alveolar concentration [MAC], respectively) were acquired. Each level increase was interleaved with a 10 min period to allow for the concentration to stabilize. A 10-min period was used due to isoflurane's low blood/gas partition coefficient allowing fast stabilization to the inspired air concentration and small step of the dosage increase (19% of the MAC for five steps and 59% of the MAC for the final step). Animals were spontaneously ventilating throughout the duration of scanning and physiological parameters (temperature, oxygen saturation, heart rate, respiration, and end-tidal CO_2) were monitored to ensure values were within normal limits. Physiological parameters across the levels are displayed in Supporting Information Figure 1. One monkey experienced abnormal breathing patterns when the isoflurane concentration was increased to 2.75% and the session was immediately terminated not allowing for data acquisition at that level. The acquisitions of two anatomical images occurred during the stabilization periods between isoflurane levels.

Data Acquisition

Data were acquired on an actively shielded 7-T 68-cm horizontal bore scanner with a DirectDrive console (Agilent, Santa Clara, California) with a Siemens AC84 gradient subsystem (Erlangen, Germany) operating at a slew rate of 350 mT/m/s. An in-house designed and manufactured conformal five-channel transceive primate-head RF coil was used for all experiments. Magnetic field optimization (B_0 shimming) was performed using an automated three-dimensional mapping procedure [Klassen and Menon, 2004] over the specific imaging volume of interest. Each functional run consisted of 150 continuous EPI functional volumes (repetition time [TR] = 2,000 ms; echo time [TE] = 16 ms; flip angle = 70°; slices = 36; matrix = 96 × 96; FOV = 96 × 96 mm^2; acquisition voxel size = 1 × 1 × 1 mm^3). Acquisition time of each scan was 5 min. EPI images were acquired with GRAPPA at an acceleration factor of 2. Every image was corrected for physiological fluctuations using navigator echo correction. A high-resolution gradient-echo T2 anatomical image was acquired along the same orientation as the functional images (TR = 1,100 ms, TE = 8 ms, matrix = 256 × 256, FOV = 96 × 96 mm^2, acquisition voxel size = 375 × 375 × 1,000 μm^3). A T1-weighted anatomical image (TE = 2.5 ms, TR = 2,300 ms, TI = 800 ms, FOV = 96 × 96 mm^2, acquisition voxel size = 750 × 750 × 750 μm^3) was also acquired.

Image Preprocessing

Functional image preprocessing was implemented in the FMRIB Software Library toolbox (FSL; http://www.fmrib.ox.ac.uk). This consisted of motion correction (six-parameter affine transformation), brain extraction, spatial smoothing (Gaussian kernel of full-width at half maximum 3 mm

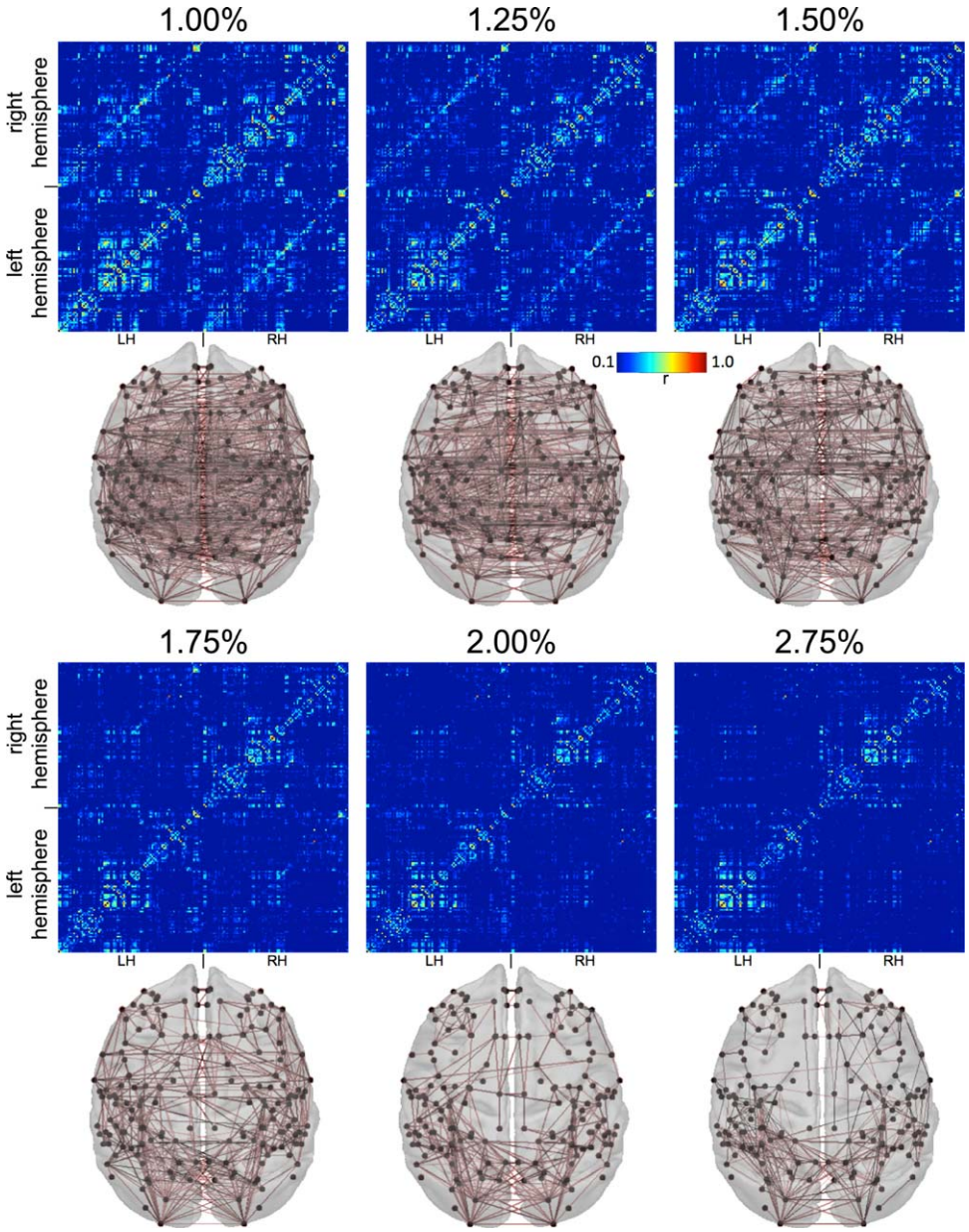

Figure 1.

Functional connectivity of macaque cortical regions across six isoflurane levels. Rows 1 and 3 show the average positive pairwise correlation matrices of regions defined using the Lewis and van Essen [2000a, b] cortical parcellation scheme. For region labels, see Supporting Information Figure 2. For negative correlations, see Supporting Information Figure 3. Below each correlation matrix (Rows 2 and 4) is the graph representation of areas (black dots, separated according to anatomical distance of each region's center of mass) and their connections (red lines, thresholded at $r \geq 0.3$). Dorsal views of the cortical surface are shown to provide approximate locations of nodes in the 2-D representation. [Color figure can be viewed in the online issue, which is available at wileyonlinelibrary.com.]

applied to each volume separately), high-pass temporal filtering (Gaussian-weighted least-squares straight line fitting with sigma = 100 s), and low-pass temporal filtering (half-width at half maximum = 2.8 s, Gaussian filter). Functional data were nonlinearly registered to the T2 anatomical (FNIRT; http://www.fmrib.ox.ac.uk/fsl/fslwiki/FNIRT), and then registered to the T1 anatomical (six degrees of freedom rigid transformation), and finally normalized

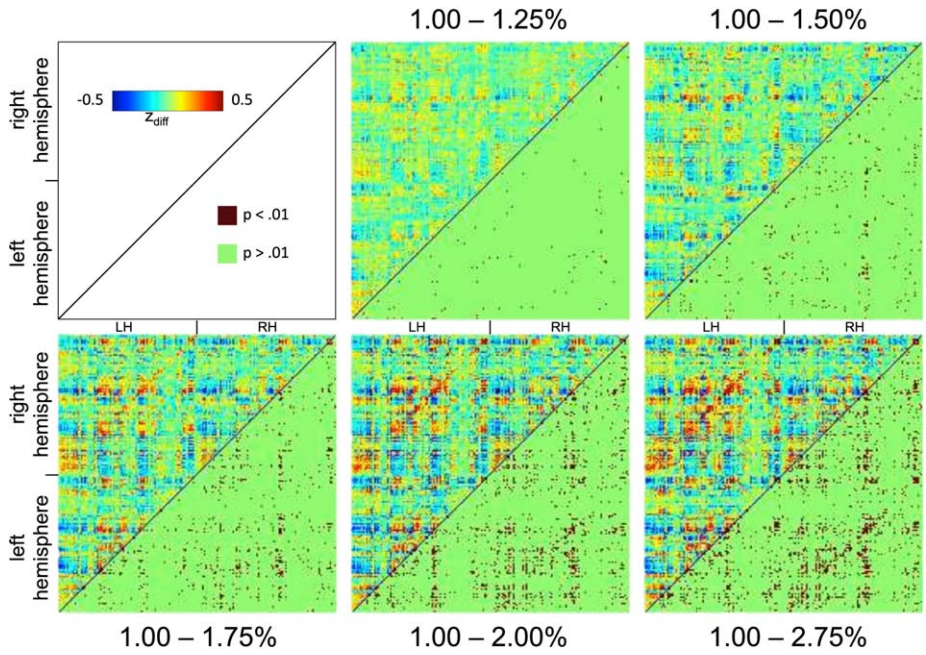

Figure 2.

Functional connectivity differences between cortical regions across isoflurane levels. The upper triangle of each plot represents the *z*-score values of that level's matrix (seen in Fig. 1) subtracted from the matrix at the 1.00% level. The lower triangle indicates whether the difference is significant ($P < 0.01$, uncorrected, two-tailed *t*-test). For region labels, see Supporting Information Figure 2. LH, left hemisphere; RH, right hemisphere. [Color figure can be viewed in the online issue, which is available at wileyonlinelibrary.com.]

(12 degrees of freedom linear affine transformation) to the F99 atlas template [van Essen, 2004; see http://sumsdb.wustl.edu/sums/macaquemore.do]. Whole brain and gray matter masks were used to define relevant voxels in which to calculate the average amplitude spectrum and total power across levels for each individual monkey.

Cortical Correlation Matrices

Connectivity matrices derived from a cortical parcellation allow for the large-scale patterns of connectivity (and anesthesia-induced changes) to be evaluated through quantification of region-to-region correlation values. They can provide global summary of changes and be assessed with graph analysis to allow quantifiable metrics of functional topology. The F99-template normalized Lewis and van Essen [2000a, b] divisions were used to define 174 (87 per hemisphere) cortical regions of interest (ROIs; see Supporting Information Fig. 2 for a list of areas and organization of the matrix). Subcortical structures were not included due to concerns related to the adequacy of an anatomically based parcellation of the small substructures, decreased signal-to-noise ratio, and a greater propensity for errors resulting from normalization. The mean time signal for each region was obtained by averaging the fMRI time series across all voxels contained within the ROI. A cross correlation matrix between all regions was then calculated for each run while partialling out the average white matter (WM) and cerebral spinal fluid (CSF) time series in addition to six motion parameters. Following a Fisher *z*-score transformation, the average of the two scans at the same isoflurane concentration was calculated. The average across all animals at each level was then calculated and the values transformed back into correlation values. The difference matrix between the five highest isoflurane levels and the 1.00% level was then calculated and significant differences ($P < 0.01$, uncorrected) using a two-tailed *t*-test were determined.

The distribution of all region–region pairs for six group-averaged matrices were calculated. The matrices were then binarized ($r \geq 0.3$, note only positive values were included) and topological graph metrics assessed using scripts from the Brain Connectivity Toolbox [https://sites.google.com/site/bctnet/; Rubinov and Sporns, 2010]. Degree centrality (the number of links connected to a node), cluster coefficient (the fraction of node neighbors that are neighbors of each other), participation coefficient (the diversity of intermodular connections of a node), distance (the shortest path between two nodes), efficiency (the matrixwise average of inverse shortest path lengths), and optimal community structure (subdivision of the matrix into nonoverlapping groups that maximizes within-group edges and minimizes the number of between group edges) were evaluated.

Seed-Based Analysis

Seed-based analysis is a univariate approach in which the time series of a priori defined ROIs are extracted and then used in a general linear model with confound regressors to derive voxelwise connectivity maps of covariance for each region. The approach allows the testing of specific hypotheses and generates easily interpretable results [Cole et al., 2010]. As demonstrated in previous papers exploring anesthesia-induced FC changes using a seed-based approach, decreased connectivity of the seed region to distributed network areas is taken to represent a breakdown in FC integrity [e.g., Boveroux et al., 2010; Liu et al., 2013a; Peltier et al., 2005; Wang et al., 2011]. Seed ROIs were defined within the prefrontal cortex (PFC), frontal eye fields (FEF), and premotor cortex area based on anatomical landmarks to explore voxelwise FC changes in the well-defined networks across anesthesia levels. The approach serves to improve the resolution of the connectivity patterns of these regions shown in the cross correlation matrices—removing the effects of averaging across multivoxel, and anatomically predefined ROIs. These regions were selected to examine ICNs composed of distributed (PFC, putatively labeled as a node of the default-mode network [DMN]; FEF, putatively labeled as a node of the oculomotor ICN); or just bilaterally homologous brain regions (premotor area, putatively labeled as node of ventral premotor ICN) based on previous work in anesthetized macaques [Hutchison and Everling, 2012; Hutchison et al., 2011, 2012a; Mantini et al., 2013; Vincent et al., 2007].

The mean time course for each ROI was extracted for every scan of each animal and the extracted time courses were then used as predictors in a model for multiple regression at the individual scan level in which nuisance covariates for WM, CSF, and six motion parameters were included. This was followed by a second level fixed-effects analysis to calculate the significantly connected voxels shared between the two scans acquired for each anesthesia level for each monkey. The group-level analysis was conducted by implementing a third-level fixed-effects analysis. A fixed-effects analysis was used due to the small number of subjects. Corrections for multiple comparisons were implemented at the cluster level with Gaussian random field theory ($z > 2.3$; cluster significance: $P < 0.05$, corrected). The group-level analysis produced thresholded z-statistic maps showing brain regions significantly correlated with each seed region across all subjects for a given level. Paired t-tests were used to compare the functional maps at different concentrations to that of the 1.00% level ($z > 2.3$; cluster significance: $P < 0.05$, corrected). To examine voxels showing a significant dose-dependent response across levels, a repeated measure one-factor ANOVA was implemented ($z > 2.3$; cluster significance: $P < 0.05$, corrected). All group results were projected from volume data to the F99 cortical surface with the CARET (http://www.nitrc.org/projects/caret) enclosed-voxel method [van Essen et al., 2001].

Independent Component Analysis

A seed-based approach tests a specific hypothesis that is dependent on those areas that are selected as seed regions. Owing to these constraints, the exploratory multivariate technique, independent component analysis (ICA) was also used to examine FC changes across isoflurane levels. The technique has been widely used to explore human FC patterns revealing robust and reproducible ICNs [e.g., Beckmann et al., 2005; Smith et al., 2009] and, more recently, has been applied to data collected from anesthetized macaques, also revealing distributed functional network connectivity [Hutchison et al., 2011; Moeller et al., 2009].

Group ICA was conducted using the GIFT software package [Calhoun et al., 2001; http://icatb.sourceforge.net]. Data from runs across all levels and animals were concatenated, and the temporal dimension of this aggregated dataset was reduced by means of principal component analysis. This was followed by spatial component estimation using the Infomax algorithm while controlling for initial algorithm conditions through the use of the ICASSO toolbox [Himberg et al., 2004] that reiterated the process 20 times. To remain consistent with model orders commonly used in human studies [Abou-Elseoud et al., 2010; Calhoun et al., 2001; Demirci et al., 2009; Smith et al., 2009] as well as our previous work in macaques [Hutchison et al., 2011], 20 components were chosen. A model order of 40 was also tested and revealed highly consistent spatial profiles of the networks that were subsequently examined. It is important to note that there are currently no well-established criteria to guide the selection of an optimal number of components for a given dataset [Cole et al., 2010]. Increasing the model order will result in a more fine-grained parcellation of networks that possibly reflects the hierarchical organization of the brains functional architecture [Abou-Elseoud et al., 2010; Meunier et al., 2010; Salvador et al., 2005; Smith et al., 2009]. As we were interested in the possible breakdown of distributed network connectivity previously shown to be susceptible to anesthesia level, a lower model order was deemed to be more appropriate.

Component time-courses and spatial maps for each level and animal were back-reconstructed, using the aggregated components and the results from the data reduction step [Calhoun et al., 2001; Jafri et al., 2008]. The mean group ICs were then calculated across both scans at each level for all animals and scaled to empirically derived z-scores. Paired t-tests were used to compare the one-sample t-test thresholded component maps at different concentrations to that of the 1.00% level ($P < 0.01$, uncorrected). To address potential concerns of concatenating data from all levels that could bias detection of network patterns at higher isoflurane levels, we also ran ICA on each level separately (model order being kept constant at 20). A multiple regression approach was then used to identify the best fitting component between the independently run levels and the corresponding group run IC network at the 1.00% level.

Dynamic State Detection

There is emerging empirical evidence that variation in FC between regions and networks that occur during a standard scan might reflect real neuronal processes that are ignored in standard resting-state investigations [Allen et al., 2014; Chang and Glover, 2010; Hutchison et al., 2013a, b; for review see Hutchison et al., 2013a]. Allen et al. [2014] have demonstrated that certain connectivity patterns can be identified across multiple subjects, dissolving and reoccurring over time. To explore the possible effects of isoflurane dose on the time-varying dynamics and state changes, the correlational analysis of the Lewis and van Essen [2000a, b] divisions was repeated with truncated versions of the ROI time series. A 30-s window (15 volumes) was advanced in increments of one time point along the entire time series and the correlation at each point recalculated for all possible shifts of the window within the 5-min (150 volume) runs. The windows containing $(174 \times (174-1))/2 = 15{,}051$ unique correlation pairs were reshaped and concatenated across all runs and animals and then, using a similar approach as Allen et al. [2014], a *k*-means clustering algorithm was applied. Note that while longer runs are more suitable for a sliding-window analysis, robust connectivity has been reported with scans of this length [Allen et al., 2014] and further, the results of two scans for each level were concatenated before *k*-means clustering was implemented. A correlation distance function was used and the algorithm was repeated 100 times with random initial mean locations to ensure optimal cluster membership. Similar to ICA, *k*-means clustering requires an a priori specification of the number of clusters (k) to group the data into. Allen et al., found that for 405 awake human subjects $k = 7$ adequately represented the data, but values were stable across a large range of k indicating that there may be no single optimal solution. Given the increased parcellation of brain regions (174 regions vs. 50) we would expect a greater number of discernable states in the present report. Indeed, assessing the average homogeneity of the windows within a cluster using Matlab's silhouette function across window sizes (5–30) revealed maximal values at $k = 30$. When examining centroids and the distribution of each centroid's membership across monkeys, it was found that this division was too fine, resulting in animal-specific clusters and some centroids that were highly similar, indicating that the k value was too high. Instead, $k = 20$ was chosen to balance cluster homogeneity and subject distribution of clusters while also providing a tractable number of states. It is important to note, that like Allen et al., different window lengths, distance functions, clustering algorithms, and cluster numbers resulted in some variation in centroid patterns, but similar results in terms of state expressions and transitions across isoflurane levels were found.

To validate the derived states, the correlation windows were randomly shuffled and clustered ($k = 20$) in the same fashion as the original data over 1,000 iterations. A distribution of graph metrics for the resulting 20,000 state patterns from the randomized data were then compared to those of the 20 states derived from the real data. Further, the state matrices were reordered by their modular structure.

RESULTS

Cortical Correlation Matrices

Figure 1 displays the average positive pairwise correlation matrices derived using the Lewis and van Essen [2000a, b] cortical parcellation scheme across the six isoflurane levels tested (for legend, see Supporting Information Fig. 2). At an isoflurane dosage of 1.00%, there are substantial intra- and interhemispheric spatial patterns evident within the matrix. Both the left and right hemispheres have strikingly similar intracortical patterns and for multiple areas there is substantial connectivity with the contralateral hemisphere that extends beyond homologous regions. Differences (between each level and the 1.00% level) and statistical comparisons are shown in Figure 2. A dose-dependent response is apparent in the contralateral hemisphere connectivity patterns where higher doses exhibit a breakdown of contralateral connectivity with areas extending beyond the homologous regions and then a prominent weakening of the homologous areas above 1.50% that is nearly abolished at 2.75% (Fig. 3). At the highest dosages tested, the intrinsic intrahemispheric connectivity is diminished in terms of strength and some connection pairs, but some of the core functional architecture (especially along the diagonal) appears to be preserved.

Figure 4 displays graph-based metrics of the binarized matrices across the six isoflurane levels. Note in cases such as the edge strength, degree, and cluster coefficient that the mean and median can be similar across different levels, however, the distribution of values can vary greatly. Broadly speaking, as isoflurane level is increased, edge strength and degree decrease, cluster coefficients become more variable, nodes showing intermediate participation coefficients ($\sim$0.2) decrease, distance increases, efficiency drops, and the community structure increase—all pointing toward a loss of coherent network topology. Region-wise, however, some areas do show preserved degree centrality between the highest and lower levels. These include regions across occipital (e.g., V1, V2d), parietal (e.g., 7a), and frontal cortex (e.g., 10m, 13a/b, 46p).

The negative connectivity patterns (see Supporting Information Fig. 3) also undergo changes across isoflurane levels. Like the positive correlation values, there is substantial underlying structure of the negative correlations with a high degree of similarity within both the left and right hemisphere that is mirrored in the contralateral connectivity pattern. The complexity of the anticorrelation

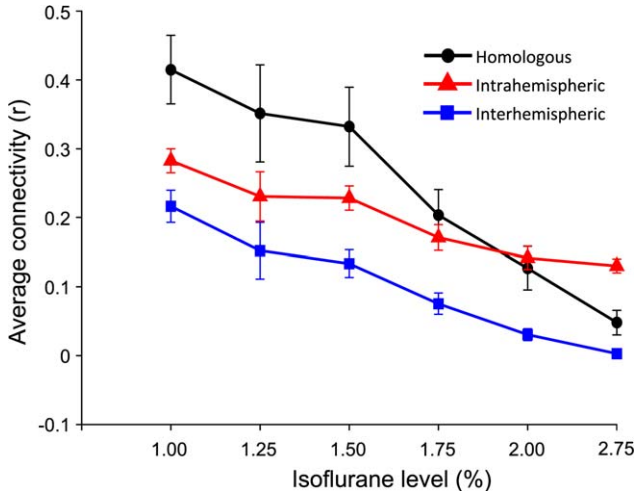

Figure 3.

Isoflurane-dependent changes in connection types. The average correlation value of homologous (black circles), intrahemispheric (red triangles), and interhemispheric (blue squares) connections (including only connections with $r > 0.1$ in the 1.00% condition) across isoflurane levels. Error bars represent standard error. [Color figure can be viewed in the online issue, which is available at wileyonlinelibrary.com.]

patterns diminishes and the apparent structure breaks down with increasing dose. Above 1.50%, many of the intrahemispheric anticorrelations approach zero, whereas contralateral connections continued to show anticorrelated connections albeit with a more simplistic structure. The changes in the cross correlation values do not appear to be directly related to variations in the amplitude spectrum or overall signal power (see Supporting Information Fig. 4). These values peak at different isoflurane dosages in different animals and can vary between runs of the same level.

Seed-Based Analysis

Seed-region analysis was used to examine potential voxelwise connectivity changes in response to isoflurane dose. Three regions were selected that have previously shown to reveal robust network connectivity in the macaque. A spherical seed (1.5-mm radius) placed in the anterior bank of the arcuate sulcus, corresponding to the location of the FEF [Bruce et al., 1985] revealed a network of regions that comprise the oculomotor network [Hutchison et al., 2012a, b; Vincent et al., 2007; Fig. 5, Column 1]. A custom seed drawn to encompass the posterior end of the principal sulcus including area 46 and parts of 9/46 of the dorsal lateral PFC [Koval et al., 2014] showed a network of regions that resemble the macaque default-mode network [Hutchison and Everling, 2012; Hutchison et al., 2011; Mantini et al., 2011; Fig. 5, Column 2]. A spherical seed (1.5-mm radius) placed at the junction of areas 3a/3b and 4, regions implicated in somato-motor-vestibular integration [Huffman and Krubitzer, 2001], revealed a set of positively correlated motor and premotor regions comprising the ventral premotor network [Hutchison et al., 2011; Mantini et al., 2013; Fig. 5, Column 3].

Across the seed-defined intrinsic networks, the FC patterns are robust and significant at 1.00% and both FC increases and decreases are evident between the 1.00% and 1.25% levels. Statistically significant differences (Fig. 6), while distributed, tend to occur to a greater degree in the hemisphere ipsilateral to the seed as well as along the cingulate cortex of both hemispheres. More profound changes begin to emerge at isoflurane levels at and above 1.50% in which there is a progressive breakdown of the core of the network, that is, the set of regions forming the canonical network pattern and in the present case, the network structure evident at 1.00%. Similar to the patterns observed when using cortical correlation matrices, there is a dramatic reduction in contralateral connectivity as well as the extent of contiguous connectivity across the cortical surface with some remaining intrahemispheric structure. Areas negatively correlated with the seed region also show a similar breakdown across levels, though in some cases are preserved at the highest dosage (e.g., visual and parietal areas of the contralateral hemisphere of the PFC seed). When evaluating regions showing dose-dependent effects across levels (see Fig. 6, bottom row), the regions comprising the core network areas show the greatest sensitivity to dose, however, there are also very distributed regions not comprising the core network that also exhibit dose-dependent effects.

Independent Component Analysis

ICA successfully (based on an ICASSO estimation) decomposed the data that were concatenated across all subjects and isoflurane levels. The resulting components closely matched those observed in previous reports [Hutchison et al., 2011; Mantini et al., 2013]. Of these, five were selected based on their spatial similarity to the networks used in the seed-based approach and to include both distributed and bilaterally homologous ICNs (Fig. 7). These were the frontoparietal (oculomotor), frontal (executive), posterior-parietal (DMN), superior-temporal (auditory), and precentral-temporal (ventral premotor) networks. The dose-dependent effects were somewhat different than observed using the hypothesis-driven seed approach. There was a very clear connectivity strength decrease across core network areas as the isoflurane dose was increased, however, the strength and extent of the connectivity notwithstanding, the general structure of the network is relatively preserved (albeit at a relatively lower z-score threshold) up until a level of 1.75%. Statistical comparisons are shown in Figure 8. The t-scores need to be interpreted with caution because corrections for multiple comparisons completely eliminated significant

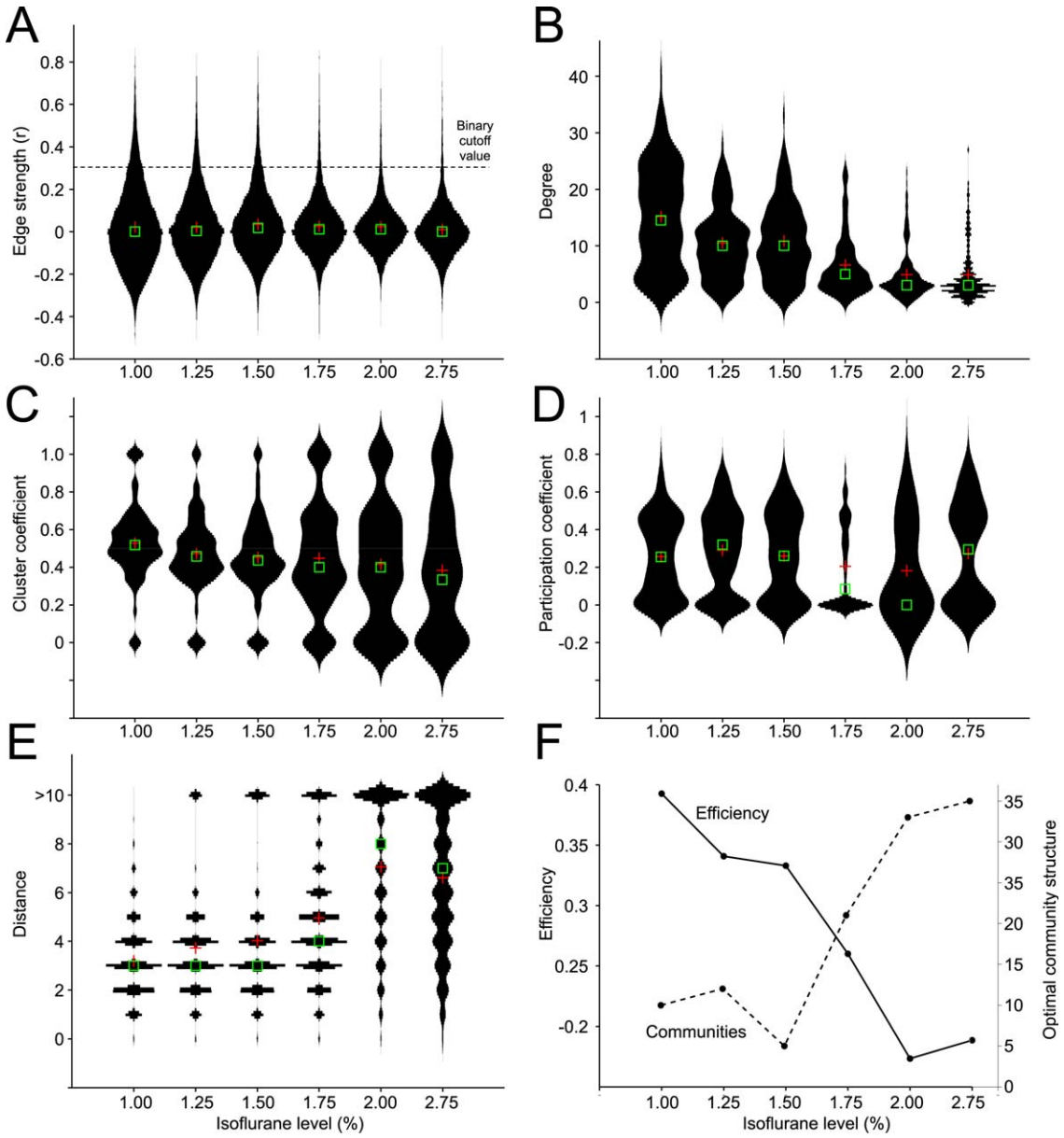

Figure 4.

Graph metrics of the functional topology of cortical connectivity matrices across isoflurane levels. Violin plots showing the distribution (black bars), mean (red cross), and median (green box) for edge strength (**A**), degree centrality (**B**), cluster coefficient (**C**), participation coefficient (**D**), and distance (**E**) are displayed. Panel F shows the efficiency (solid line, left axis) and optimal community structure (dashed line, right axis). Metrics were computed on binarized matrices ($r \geq 0.3$). [Color figure can be viewed in the online issue, which is available at wileyonlinelibrary.com.]

differences (possibly owing to the small sample size used in the study) and, were therefore, not implemented. The distributed networks (Columns 1–3) showed the most significant breakdown of structure at higher isoflurane levels, though even at 2.75%, some the core areas of the frontoparietal network can still be observed. ICNs comprising strictly bilateral homologues (Columns 4 and 5) show the same strength and spatial extent dose responses, as distributed networks. At 2.00%, the preserved bilateral connectivity makes these networks still identifiable, however, at our next recorded dosage (2.75%) there is, not surprisingly, a near complete breakdown of the ICN. These results are similar when ICA was run separately for each isoflurane level (see

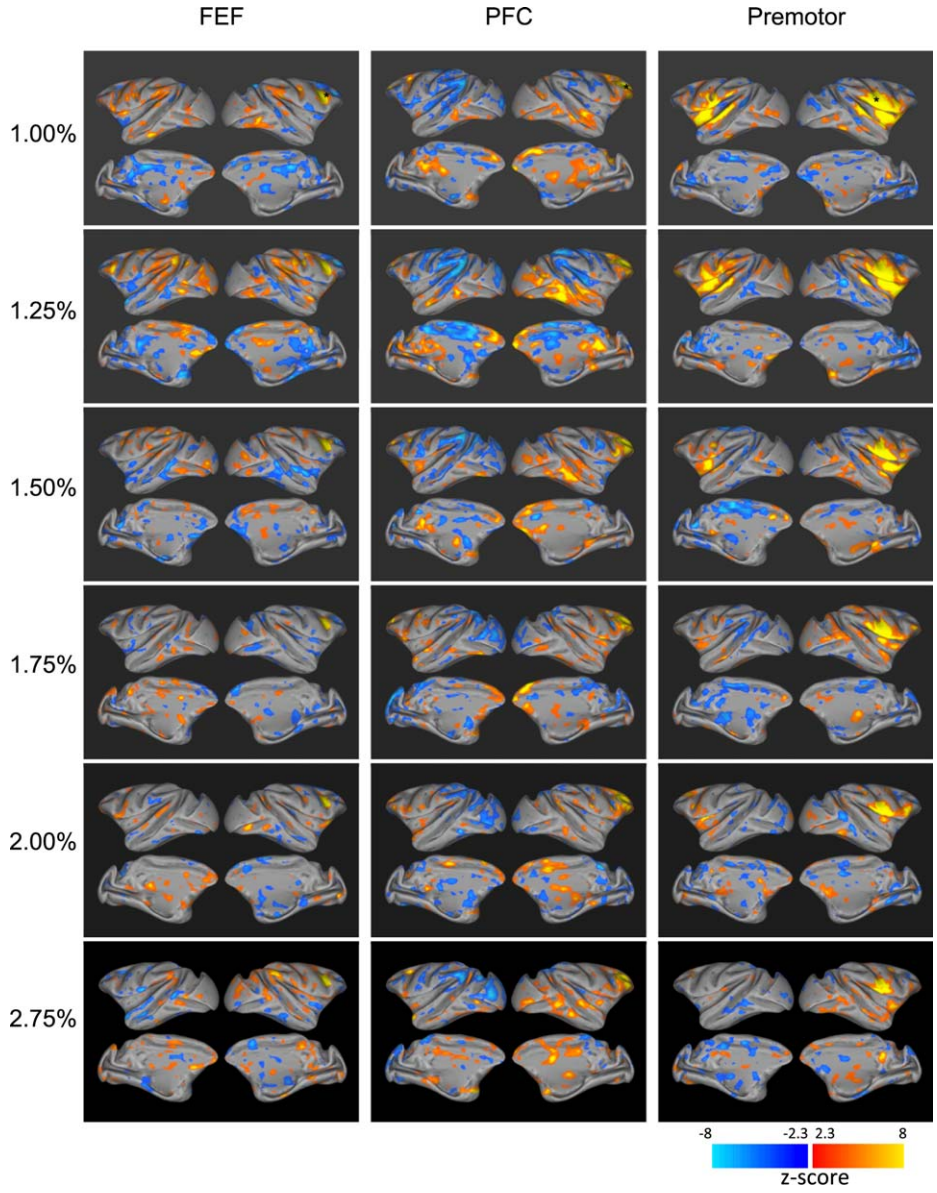

Figure 5.

Whole brain, group-averaged functional connectivity of seed regions (columns) placed within areas corresponding to the frontal eye field (FEF; left column), prefrontal cortex (PFC; middle column), and motor area (Premotor; right column) across isoflurane levels (rows). Color overlays represent thresholded z-score maps ($z > 2.3$; cluster significance: $P < 0.05$, corrected) overlaid on the lateral and medial views of both hemispheres on partially inflated cortical surfaces of the F99 template brain. For statistical comparisons and overall dose-dependent effects, see Figure 6. Black asterisks indicate the location of the seed regions. [Color figure can be viewed in the online issue, which is available at wileyonlinelibrary.com.]

Supporting Information Fig. 5). Greater connectivity decreases are, however, apparent at and above the 2.00% level for networks other than the frontal network. Changes in the max r^2 value from the multiple regression analysis used to identify the component best matching that at the 1.00% level of the concatenated data reflect the loss of network structure that occurs as dose increases.

Dynamic State Detection

k-means clustering ($k = 20$) clustered the data into 20 centroids (Fig. 9, also see Supporting Information Fig. 6 for matrix representations) that showed a diffuse range of state patterns. Permutation testing using randomized ordering revealed that the topological properties

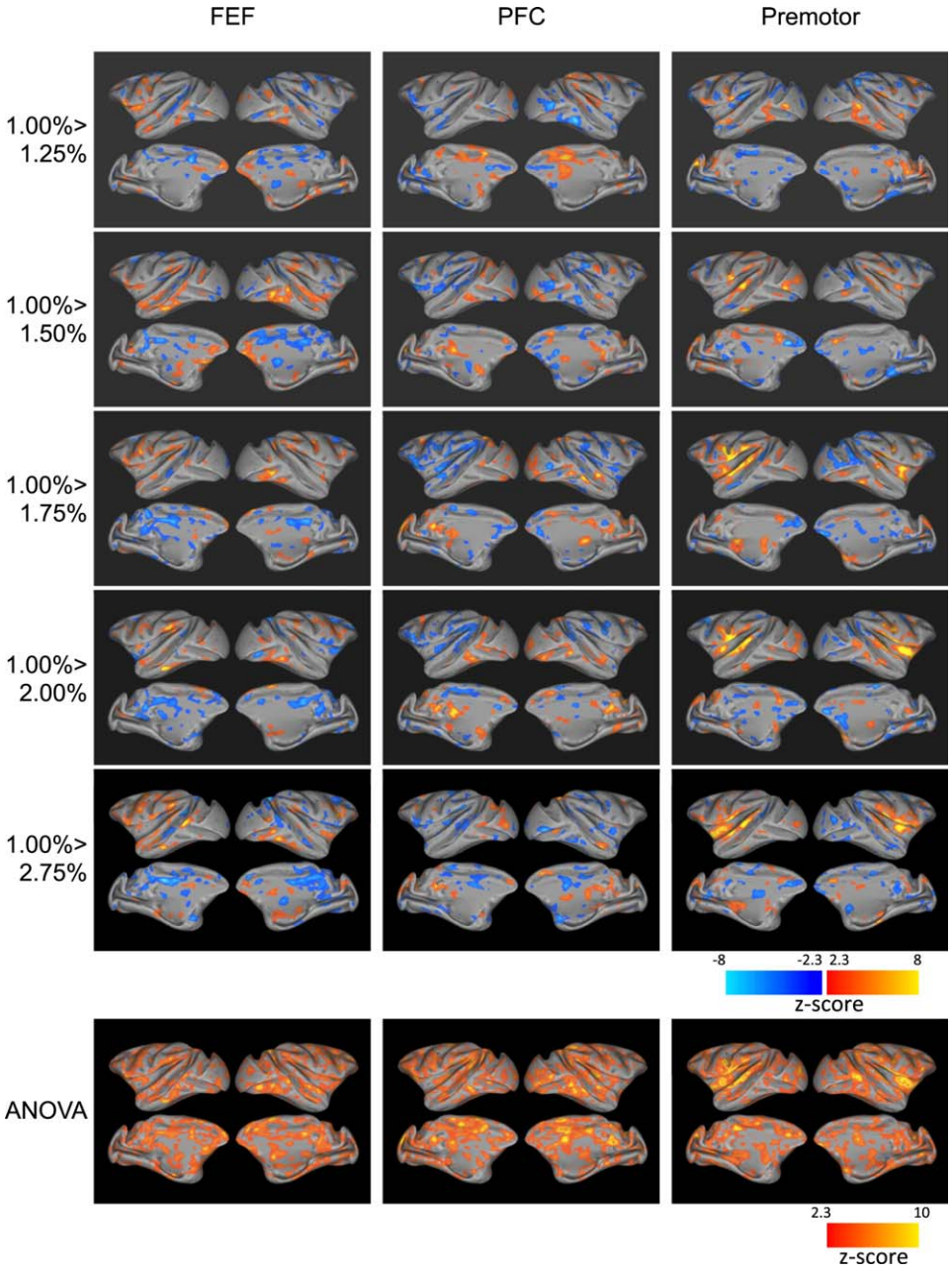

Figure 6.

Statistical comparisons of seed-based analysis results shown in Figure 5. Color maps of the top rows represent thresholded *z*-score maps following paired *t*-test comparisons of each isoflurane level and the 1.00% isoflurane condition ($z > 2.3$; cluster significance: $P < 0.05$, corrected) for seed regions (columns) placed within areas corresponding to the frontal eye field (FEF; left column), prefrontal cortex (PFC; middle column), and primary motor area (right column). The bottom row shows voxels with a significant dose-dependent response following a repeated measure one-factor ANOVA ($z > 2.3$; cluster significance: $P < 0.05$, corrected) Maps are overlaid on the lateral and medial views of both hemispheres on partially inflated cortical surfaces of the F99 template brain. [Color figure can be viewed in the online issue, which is available at wileyonlinelibrary.com.]

(average clustering coefficient, participation, distance, or the overall efficiency) of the 20 states to be significant ($P < 0.000$; Supporting Information Fig. 7). There was overlap between real and randomized states in their optimal community structure (Supporting Information Fig. 7B) possibly owing to the preserved degree values, however, when

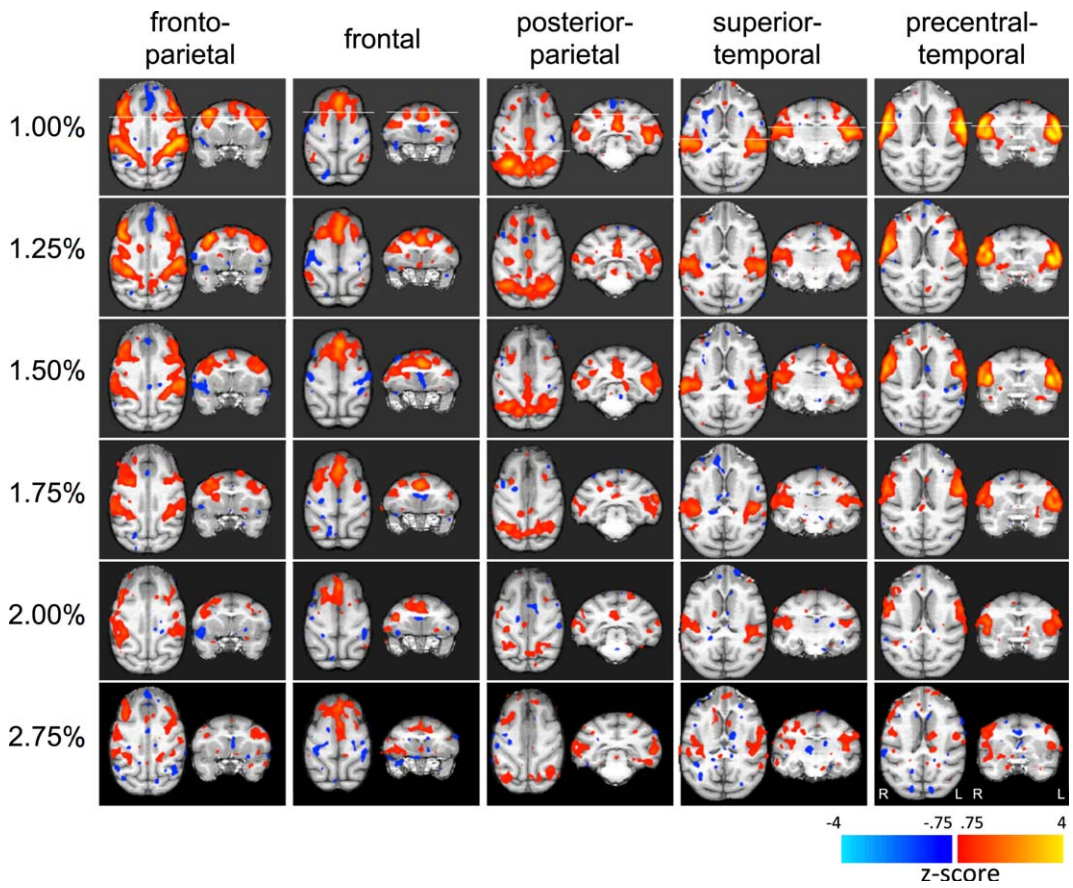

Figure 7.

Select macaque networks (columns) across isoflurane levels (rows) derived using group-ICA. Overlaid color maps represent thresholded z-scores that are displayed on coronal and transverse views of the F99 template brain. For statistical comparisons, see Figure 8. [Color figure can be viewed in the online issue, which is available at wileyonlinelibrary.com.]

organizing centroids based on their modularity, structure is only apparent in the original state patterns (Supporting Information Fig. 8). When taken together, the results suggest that the state patterns are not simply a byproduct of the clustering algorithm forcing a solution—as the patterns demonstrate more physiologically plausible topology characteristics.

The distribution of state occurrence across all animals and levels is shown in Figure 10A. Figure 10B displays the distribution of the states across each isoflurane level and demonstrates that all states do not occur to equal proportion across levels. To further examine this finding, Figure 9 indicates the correlation of the number of occurrences of each centroid/state at each isoflurane dosage. Negative values indicate states that occur less frequently as the isoflurane dose is increased, while positive values indicate states that occur more frequently. The data show that many of the more structured and complex states occur less frequently as isoflurane dose is increased (e.g., 2, 12, and 17), whereas the states that could be considered less specific and more "noisy" increase with an elevated anesthetic dosage (e.g., 19 and 20). To further examine dose-dependent effects of the dynamic state properties, Figure 11A displays the average number of unique states that are expressed as a function of the isoflurane level. There is actually an increase in the average state expression for monkeys anesthetized at 1.25% and 1.50% compared to the 1.00% level, and up until 1.75%, the animals tend to express 8–9 states across the scanning period (2 × 5 min) regardless of the dosage. A notable reduction in state expression is only evident at 2.00%. It is important to note that even at 2.75%—a level that would be considered profoundly deep anesthesia there are still approximately four unique states expressed across the scanned level. More closely related to isoflurane dosage was the number of state transitions (which could be inversely expressed as dwell time of a current state) that occur throughout the scan. This showed a near linear relationship with dose (Fig. 11B) so that as the dosage is

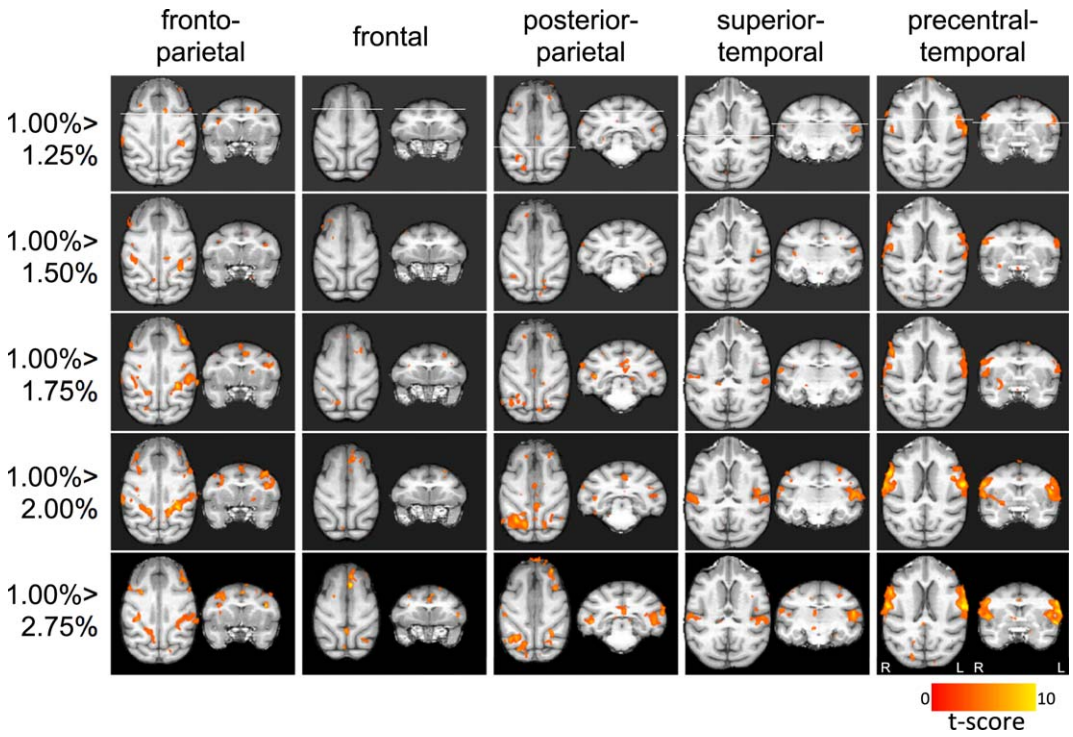

Figure 8.

Statistical comparisons of group-ICA based analysis results shown in of Figure 7. Color maps represent thresholded z-score maps following paired *t*-test comparisons of each isoflurane level and the 1.00% isoflurane condition ($z > 2.3$; cluster significance: $P < 0.05$, corrected) for select macaque networks (columns). Maps are overlaid on coronal and transverse views of the F99 template brain. [Color figure can be viewed in the online issue, which is available at wileyonlinelibrary.com.]

increased, the cortex tends to stay in the current state longer and does not transition to other states as frequently.

DISCUSSION

The goal of the present study was to examine the dose-dependent effects of isoflurane on the FC of the macaque cortex. Many of the previous imaging studies using PET or fMRI to explore anesthesia's effects assessed the difference between consciousness and unconsciousness [Alkire et al., 1997, 1999; Boveroux et al., 2010; Deshpande et al., 2010; Greicius et al., 2008; Liang et al., 2012; Martuzzi et al., 2010; Moeller et al., 2009; Peltier et al., 2005; Schrouff et al., 2011] and typically restricted their evaluation to a limited number of ICNs. Here, we explored the changes that occur at multiple discrete levels beyond the point of what is typically defined as unconsciousness (unresponsive) across whole brain patterns and multiple networks. While this approach does not allow for the elucidation of the neural correlates related to the transition to (un)consciousness, it does provide insight into features as the general anesthesia deepens. Overall, the results pointed toward a graded effect of the anesthetic on the large-scale spatial and temporal functional architecture.

Isoflurane

Isoflurane is a commonly used anesthetic in RS-fMRI (and other neuroimaging) investigations of rodents [Hutchison et al., 2010; Kannurpatti et al., 2008; Liu et al., 2011; van Meer et al., 2010; Wang et al., 2011] and nonhuman primates [Hutchison et al., 2011; Mars et al., 2011; Shmuel and Leopold, 2008; Teichert et al., 2010; Vincent et al., 2007], serving to eliminate motion effects, physiological stress, and training requirements. It is often selected as the anesthetic agent of choice because of its robustness, suitability for survival studies, rapid induction and recovery, low cost, as well as the nonobligatory requirement for mechanical ventilation; though it also has co-occurring effects on cerebral blood flow (CBF), blood volume (CBV), and metabolic rate (reviewed in Masamoto and Kanno, 2012; discussed below) that must be considered and has motivated the use of other anesthetic regimens such as α-chloralose [Lu et al., 2007; Majeed et al., 2009], medetomidine [Pawela et al., 2008; Zhao et al., 2008], propofol [Matsui et al., 2011], and ketamine/xylazine

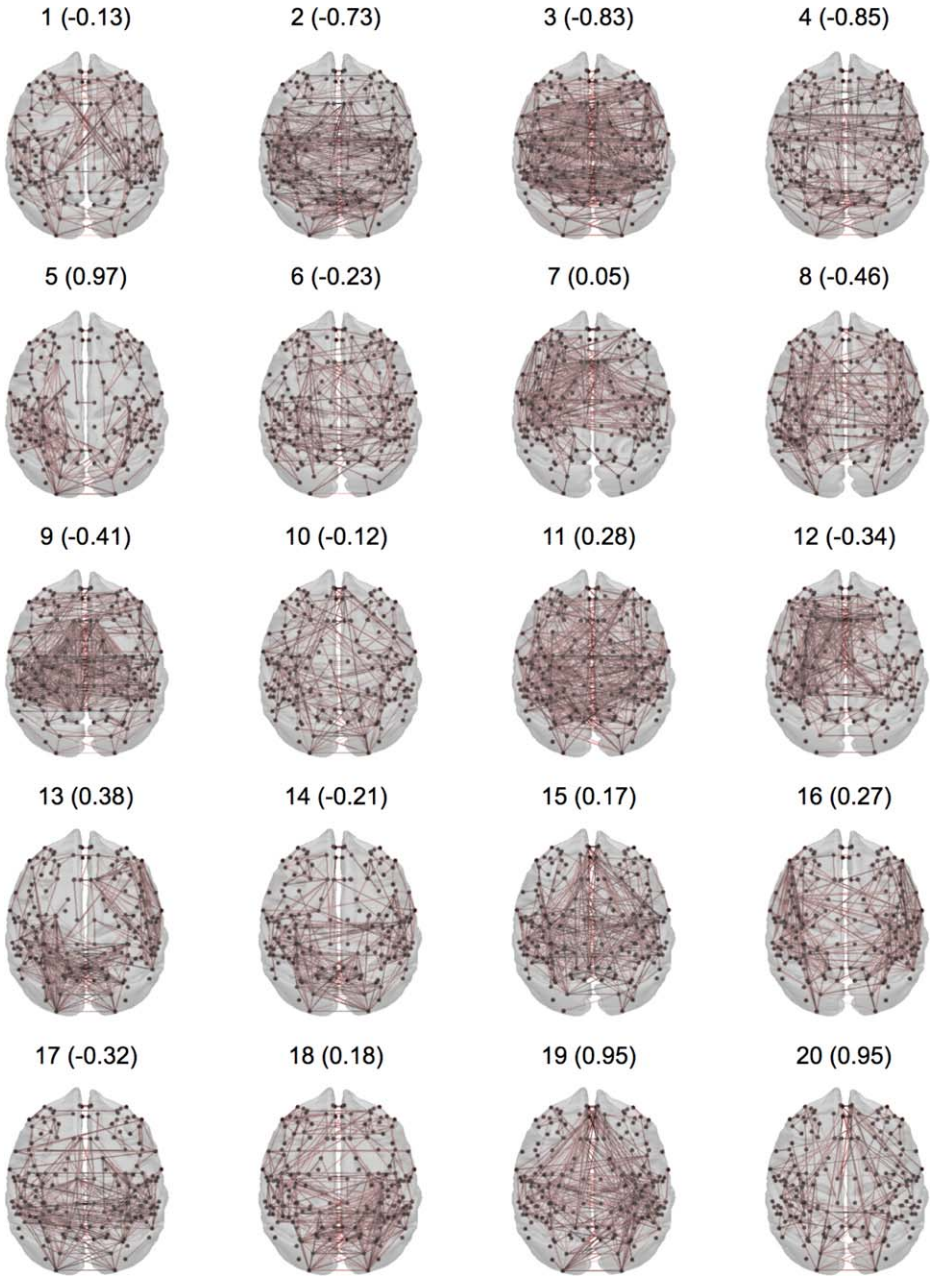

Figure 9.

Graph representations of cluster centroids following a *k*-means clustering ($k = 20$) of all runs and animals. The number indicates the cluster number corresponding to the histograms in Figure 10. The number in parentheses indicates the correlation of the number of occurrences of that cluster and the isoflurane level. For full matrices, see Supporting Information Figure 6. [Color figure can be viewed in the online issue, which is available at wileyonlinelibrary.com.]

[Hutchison et al., 2010]. Isoflurane is used in human surgical settings, but in some cases it has been replaced with other agents, such as sevoflurane, that have similar mechanisms of action, but fewer irritant respiratory properties. Isoflurane has been shown to target multiple membrane proteins including major potentiation of $GABA_A$, glycine, two-pore-domain potassium channel, $5\text{-}HT_3$ (serotonergic), and kainate receptors as well as significant inhibition

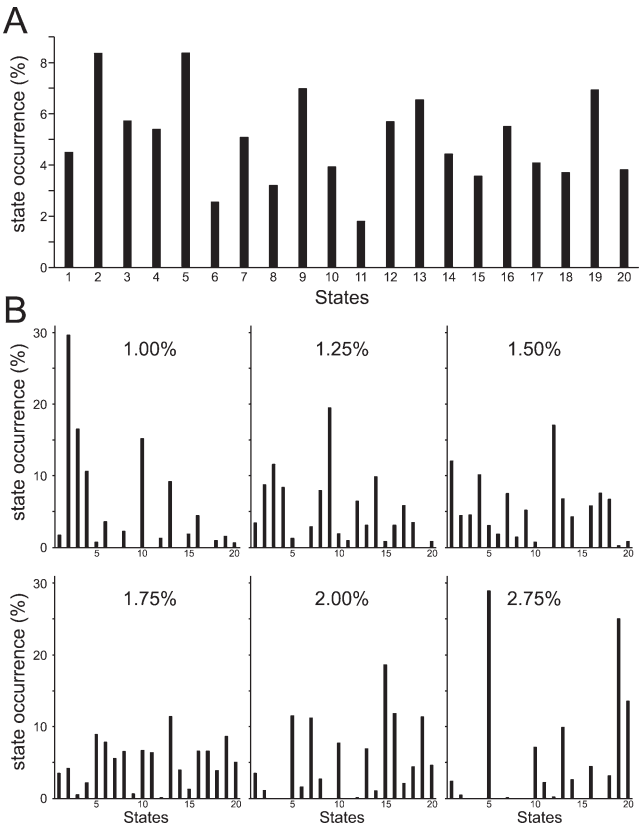

Figure 10.

Dynamic state distributions of isoflurane anesthetized macaques across all runs (**A**) and at each isoflurane level (**B**). The spatial patterns of the 20 states (*x*-axis) are shown in Figure 9 and Supporting Information Figure 6. The distribution is expressed as a percentage of their occurrence.

of inwardly rectifying potassium channels and AMPA receptor types with minor inhibition of NMDA, voltage gated potassium channels, nicotinic and muscarinic acetylcholine receptors [for review, see Franks, 2008]. In humans, below 1 MAC [1.2%; Nickalls and Mapleson, 2003], isoflurane-induced unconsciousness is typically characterized by slow wave activity in the electroencephalographic recordings. At levels above 1 MAC, burst suppression can occur consisting of periods of high-amplitude neural activity (burst) alternating with epochs of quasiperiodically isoelectric quiescence (suppression) that becomes progressively longer as the dose is increased [Swank and Watson, 1949]. These patterns are most prominent above 1.5 MAC and electrical silence is often observed at 2–2.5 MAC [Hoffman and Edelman, 1995]. MAC, the concentration of anesthetic needed to prevent motor responses in 50% of subjects in response to surgical stimulus (typically an incision), is by its criteria, not a definitive measure. The value and associated electrical activities can be difficult to predict and further confounded by age or health conditions. Dose-dependent assessment of electroencephalography (EEG) patterns under isoflurane anesthesia in nonhuman primates are scarce. The MAC of isoflurane has been estimated to be 1.28% [Tinker et al., 1977] within a similar range as human subjects. Vincent et al. [2007] has shown that light isoflurane anesthesia (0.90–1.00%; 0.70–0.78 MAC) results in continuous low-frequency activity that at moderately deep anesthesia (1.25–1.50%; 0.97–1.17 MAC) turns to burst suppression. The range of values used here likely spanned periods of slow wave activity to near complete burst suppression approaching neural silence.

Interruption of Information Integration

While a number of theories related to anesthesia's mechanism of action exist, many converge on integration as the critical element that is affected. The information integration theory of consciousness posits that consciousness is directly linked to the capacity of the brain to integrate information across distributed brain areas [Tononi, 2004]. Evidence from different modalities suggests that anesthetic agents likely disrupt this functional communication causing dissolution of meaningful information transfer [for review, see Alkire et al., 2008; Hudetz, 2006]. The alteration of cognitive communication could take several forms including changing the balance of excitation and inhibition, suppressing recurrent feedback signaling, and directly altering thalamo-cortical or cortico-cortical connectivity [Boveroux et al., 2010; Martuzzi et al., 2010; Mhuircheartaigh et al., 2010; White and Alkire, 2003].

There is no consensus in the literature in regards to how the loss of integration will be manifested in FC measures of spontaneous BOLD fluctuations. The dissolution of integration has been interpreted from observations of nonuniform breakdown of large-scale synchronization between brain regions in which higher anesthetic dosages result in brain areas that tend to be organized into independent modules with decreased correlation patterns with other regions [Deshpande et al., 2010; Lu et al., 2007; Peltier et al., 2005; Vincent et al., 2007]. Conversely, other empirical studies (even some using the same anesthetics) have shown that an increasing anesthetic dose causes a global loss of functional segregation/specialization resulting in FC maps that display a decreased specificity, with regions becoming more homogeneously connected to each other [Kalthoff et al., 2013; Liu et al., 2011, 2013b; Vincent et al., 2007]. The present findings add support to the former notion. We observed dose-dependent changes in the strength, spatial extent, and topological properties of FC patterns when examining broad cortical connectivity patterns of pairwise correlations (Figs. 1–4), specific region FC maps (Figs. 5 and 6), or isolated networks following an exploratory ICA (Figs. 7 and 8). Distributed and higher order areas tended to be the most susceptible to isoflurane dose, particularly regions in the contralateral hemisphere. This is in agreement with previous work showing that

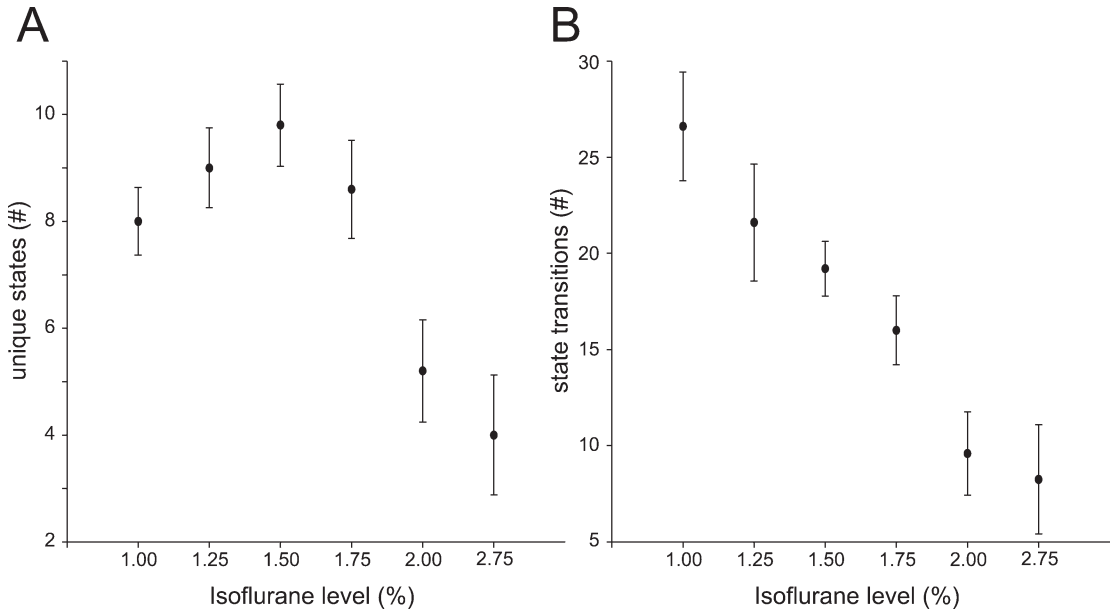

Figure 11.
The average number of states expressed (**A**) and state transitions (**B**) across animals as a function of isoflurane level.

anesthesia exerts effects differentially across functional networks [for review, see Bonhomme et al., 2012]. The functional connections between bilateral homologues, which typically exhibit the most robust and stable FC, also lessened and eventually broke down, though some homologous connectivity was still evident at higher levels in the ICA. While weak and spatially altered, the bilateral FC could be attributed to ICA's better ability to remove noise and capture weak temporal relationships, especially among lower order sensory areas, but further investigation also suggested some of the patterns are partially driven by running the ICA with all level concatenated together. Our initial expectations were that there would be dissolution of ICNs at the higher isoflurane doses ($\geq$2.00%) due to increased periods of neural quiescence associated with burst suppression. This would result in spontaneous BOLD fluctuations that approximate meaningless noise, resulting in spatial decoherence in the brain [Peltier et al., 2005; Wang et al., 2011]. However, while the patterns were substantially altered, there is nonetheless still some apparent structure that remains even at higher isoflurane levels—this is especially evident in the frontal network.

It has been suggested that the variability in large-scale neural patterns shrinks (equating to a loss of information) during deep anesthesia, either as a consequence of the loss of integration or as an independent phenomenon. In the case of isoflurane, this would theoretically lead to a stereotypic burst-suppression pattern with only two possible states, "on" or "off" [Alkire et al., 2008]. Liu et al. [2011] suggested that the decreased FC specificity patterns as a function of dose observed in their study of isoflurane anesthetized rats offered evidence of a collapse of the repertoire of cortical activity pattern and thus of information. However, standard static based measures may not represent the ideal approach to test this hypothesis, as it is difficult to assess information content from a single averaged correlation value between regions.

Anesthesia's Effect on the Dynamic Functional Repertoire

Here, we used a dynamic FC approach to determine if the functional repertoire and dynamic reconfigurations of spontaneous brain states decrease at levels past the point of anesthesia-induced unconsciousness. While analysis strategies and interpretation of temporal FC changes are still in their relative infancy, studies are emerging that support that these changes are not solely random phenomena [Chang and Glover, 2010; Handwerker et al., 2012; Hutchison et al., 2013b; Jones et al., 2012; Keilholz et al., 2013; Kiviniemi et al., 2011], but have a significant neural contribution [Chang et al., 2013; Tagliazucchi et al., 2012], and form reproducible states [Allen et al., 2014; for review; see Hutchison et al., 2013a]. The notion that functional connections exhibit dynamic patterns is intuitive across other disciplines and is considered a fundamental requirement for the brain to dynamically integrate, coordinate, and respond to internal and external stimuli across multiple time scales [for reviews, see Rabinovich et al., 2012; von der Malsburg et al., 2010]. Our results pointed toward a decreased number of states at

high dosages of isoflurane anesthesia. At moderate dosages (1.00–1.50%), however, there was an increase in state expression that would not have been initially predicted. The expansion of the state repertoire could correspond to the increased root mean square of the amplitude and bursts of alpha and beta activity that have been observed in patients and animals under isoflurane anesthesia at levels near 1 MAC [e.g., Detsch et al., 2000; Rampil et al., 1988]. Future work will be necessary to relate these two phenomena and verify the increase in a larger group of animals. The average number of states expressed per animal at these levels (~8–9) may not represent the complete repertoire of brain states that occur in awake conditions. Differences between awake and anesthesia states assuming static connectivity have reported significant FC differences [Deshpande et al., 2010; Liu et al., 2011, 2013b; Lu et al., 2007; Peltier et al., 2005; Vincent et al., 2007; Wang et al., 2011] and likely these are indicative of underlying changes to the dynamic repertoire. However, robust patterns are still evident under anesthesia that resemble those in awake conditions, suggesting that some of these state patterns will be expressed in both conditions. A similar analysis strategy (albeit with fewer regions and the inclusion of some subcortical structures) reported seven consistent states in awake human subjects [Allen et al., 2014] so the range reported here is not disparate. Future studies are needed to determine the complete range of FC states across multiple conditions including awake and anesthetized states. Importantly, even at suprathreshold dosages, there are more than two states expressed as was initially expected above 2.00%. Besides the expression of unique states, Flohr [1995] has stated that, "the occurrence of states of consciousness causally depends on the rapid formation (and disintegration) of complex representational structures." From Figure 11, it is clear that there is a tight relationship between transitions and isoflurane levels so as the dose is increased the number of state transitions decrease and the amount of time spent within a state increases.

When viewing spontaneous FC dynamics as the result of noise-driven transitions between multistable attractor states in a global attractor model [Deco and Jirsa, 2012; Deco et al., 2009; for review, see Deco et al., 2011], decreased transitions/increased dwell times could be interpreted as a result of several key changes. The decreased repertoire of states (at higher dosages) as well as a change in the frequency (or emergence) of states could suggest an altered multistable state region that is explored, a decrease in entropy, or possibly a move away from the edge of bifurcation—a point necessary to allow exploration of the state space [Deco and Jirsa, 2012; Deco et al., submitted]. The increased dwell time could indicate an overall decrease in the "noise" as a result of the isoflurane-induced quiescence, limiting the available "kinetic energy" necessary to explore possible functional architectures [Ghosh et al., 2008]. It also cannot be ruled out that isoflurane results in more robust attractor states, states that are expressed, or the dissolution of more closely related states, making it more difficult to transition to neighboring attractors. Based on the idea that the state fluctuations could represent predictive functional characterizations as in a Bayesian framework [Körding and Wolpert, 2006; Pouget et al., 2003; Sadaghiani et al., 2010], in which ongoing cortical activity represents a continuous top-down prediction or expectation [Buckner and Vincent, 2007; Engel et al., 2001], it is possible that the breakdown of interpretable sensory input, a lack of cortical feedback, or general interruption of integration hinders the system and reduces the predictive ability of the brain and subsequently, the relevant transitions. Future work examining the global effects of anesthesia on the well-developed large-scale brain models of spontaneous activity will be needed to better understand this phenomenon and address these hypotheses.

Confounds and Considerations

Across resting-state fMRI anesthesia investigations, concerns exist that the neurovascular decoupling that occurs at higher dosages will confound observations of potential neural changes [for review, see Masamoto and Kanno, 2012]. Traditional analysis approaches are particularly susceptible to these global effects in which values can be artificially increased or decreased compared to awake or lightly anesthetized states as CBF and CBV shift with no underlying change in neural activity. A complete understanding of vascular coupling in awake states is still tenuous [Goense and Logothetis, 2008; Logothetis et al., 2001; Logothetis, 2002; Shmuel et al., 2006, for review, see Logothetis, 2008] and the effects across anesthetic types and levels are even more equivocal. The hypotensive effects of higher isoflurane dosages can cause decreased CBF and oxygenation (with concomitant hypercapnia) and vasomotor waves leading to decreased detectability/specificity of BOLD signal fluctuations, and further, the vasodilatory effects of isoflurane have the potential to decrease the BOLD signal power, artificially lowering correlation values. However, a decrease in blood pressure has also been shown to increase FC through enhancement of low-frequency amplitudes [Kannurpatti et al. 2008] and reduction of the relative power of the faster BOLD oscillations [Kiviniemi et al., 2005]. These effects require that studies examining BOLD signals under anesthesia that may uncouple the neural activity and hemodynamics be interpreted with caution as results may be confounded by changing and complex interactions.

Monitoring was used to ensure physiological variables were within a normal range throughout the scan sessions. However, the measures were not continuously recorded to allow for accurate regression of time series and their derivatives. Periodic assessment of O_2 saturation, heart rate, end-tidal CO_2, and respiration rate did not indicate significant ($P > 0.05$, two-tailed t-test; Supporting Information Fig. 1)

group level differences between levels. The sample size used in the study was small, however, and it is likely changes in vital signs impacted the results. Optimally, characterization of anesthetic depth and physiologic response would include assessment of blood pressure, electrocardiography, and EEG. End-tidal anesthetic concentration is less informative as isoflurane has a relatively low blood/gas partition coefficient that causes rapid induction to the inspired concentration [Cromwell et al., 1971] that can be reliably predicted from the set vaporizer level [Liu et al., 1995]. Depth of anesthesia could also be evaluated through assessment of reflexive responses; however, the animal's position in the scanner bore makes this difficult.

Analysis of the amplitude spectra and average signal power of grey matter voxels across isoflurane levels (Supporting Information Fig. 4) did not reveal a clear trend. Variability of the Fourier transform and total power was evident between scans of the same level within subject and across animals. While power decay was evident in some cases (e.g., Case M4), there are levels in which power was higher than that at lower dosages (e.g., Case M6). Studies combining fMRI with electrical recordings will be critical to delineate the vascular and neural effects contributing to these changes. Simultaneously recorded EEG–fMRI [Liu et al., 2013a (interleaved design); Vincent et al., 2007] and separate EEG and fMRI acquisitions under similar parameters [Lu et al., 2007] have suggested a close relationship between changes in electrical activity and hemodynamic and FC changes, however, more work is needed. The current seed-based and ICA results must be interpreted with this caveat, however, the specificity of the breakdown does not point solely toward vascular effects. Further, WM and CSF values were also partialled out of the seed-based analyses, the latter composed of virtually identical frequency components as the global signal. ICA can isolate contaminant sources and was run on the entire concatenated data, limiting global signal effects. The effects of higher levels of anesthesia on dynamic FC patterns are likely faithful to the underlying neural activity. Though some variability exists, anesthesia produces moderately uniform effects on neurovascular coupling across cortical brain areas [Li et al., 2013; Qiu et al., 2008]. As we observed changes in the time-varying states in terms of expression, distribution, and timing, a property that would not be changed by a global neurovascular effect, it points toward changes of a neural origin.

The animals used in this study were naïve and not trained to remain still in the scanner environment. As such, we were not able acquire an awake baseline scan, restricting our discussion to graded levels of anesthesia following loss of consciousness and not the transition between consciousness and unconsciousness. This limitation also extends to those isoflurane values below 1.00% in which reliable anesthesia in the macaque is difficult to maintain (without agents) resulting in animals regaining consciousness, stress responses, and motion artifacts. However, valuable conclusions can still be drawn from the present results. It is well-established in a clinical setting that as the dose of general anesthetic increases, subjects experience amnesia, then sedation progressing to unconsciousness, and finally, immobility and areflexia, typically having invasive surgeries performed at or before burst suppression levels [Brown et al., 2010]. Researchers exploit the properties of subanesthetic doses to affect selected components of consciousness such as memory, attention, pain, or emotional processing. Little of the current research, however, examines points beyond moderate to deep levels of anesthesia. Consciousness has been postulated to be graded, being progressively broken down or "dimmed" by anesthesia as opposed to being an all-or-none phenomenon, that is, turned on and off [Alkire et al., 2008; Hudetz, 2006; Tononi, 2004]. Our results indicate that there are progressive phases that exist in deep anesthesia that occur before complete isoelectricity. While there may be nonlinear and dramatic changes that occur at the point of induction it seems that the changes occur more gradually once unconsciousness is induced. Also, it appears that spontaneous neural activity can still be highly synchronized over different brain regions at high dosages of isoflurane with a progressive breakdown that might follow the anatomical connections in terms of strength and distance, where strong neighboring intracortical connectivity follows robust intrahemispheric homologues, that proceeds loss of more distributed intra- and contrahemispheric connections as anesthesia deepens.

Appropriate Isoflurane Levels for Future Studies

As mentioned above, anesthesia presents an obvious confound for nonhuman primate resting-state investigations, however, the benefits, including allowing extended, motion-free acquisition in naïve animals, continue to motivate its use. It is evident that coherent networks persist in unconsciousness, but currently, there is no consensus on a suitable range to evaluate FC or whether it is acceptable to implement optimized levels for individual subjects. Seminal work investigating FC patterns in the isoflurane anesthetized macaque [Vincent et al., 2007] found that, while 0.80–1.10% ("light anesthesia," slow continuous EEG activity) was associated with somewhat stronger and more system-specific correlations in the oculomotor and somatomotor networks, 1.20–1.50% ("deep anesthesia," burst suppression pattern) FC maps also showed all of the core regions of the networks and subsequently grouped data across levels. A human study reported a breakdown of interhemispheric connectivity of homologues in the DMN at a sevoflurane concentration of 1.00% [Peltier et al., 2005] that would suggest the dose to be too high for assessment of higher order ICNs, however, the finding was not reproduced in a later study that found bilateral connectivity at the same dosage across multiple networks [Martuzzi et al., 2010]. Taken together with the current findings, including the dynamic FC results, it is reasonable to conclude that

an isoflurane level at 1.50% (a level with preserved CBF autoregulation [Eger, 1984; Li et al., 2013] and below is a suitable range for most nonhuman (and likely human) resting-state investigations though this value will nevertheless be dependent on the precise question of interest.

CONCLUSIONS

Examination of dose-related changes in FC patterns of the macaque pointed toward both widespread and gradual spatial and temporal alterations that occur beyond the typically defined endpoint of consciousness. The results suggest that changes continue to occur past the loss of consciousness and the graded process is closely linked to the ongoing formation/dissolution of discriminable state patterns. While many open questions and future directions remain including the use of a larger cohort of subjects, the present work continues to support the use of RS-fMRI as a suitable method with which to characterize large-scale alterations related to pharmacological measures and the use of dynamic FC measures will likely serve to offer more physiologically meaningful understanding of these changes.

ACKNOWLEDGMENTS

The authors thank S. Hughes for technical assistance and the anonymous reviewers for suggestions that significantly improved the manuscript. The authors declare no conflicts of interest.

REFERENCES

Abou-Elseoud A, Starck T, Remes J, Nikkinen J, Tervonen O, Kiviniemi V (2010): The effect of model order selection in group PICA. Hum Brain Mapp 31:1207–1216.

Alkire MT, Haier RJ, Shah NK, Anderson CT (1997): Positron emission tomography study of regional cerebral metabolism in humans during isoflurane anesthesia. Anesthesiology 86:549–557.

Alkire MT, Pomfrett CJ, Haier RJ, Gianzero MV, Chan CM, Jacobsen BP, Fallon JH (1999): Functional brain imaging during anesthesia in humans: Effects of halothane on global and regional cerebral glucose metabolism. Anesthesiology 90:701–709.

Alkire MT, Hudetz AG, Tononi G (2008): Consciousness and anesthesia. Science 322:876–880.

Allen EA, Damaraju E, Plis SM, Erhardt EB, Eichele T, Calhoun VD (2014): Tracking whole-brain connectivity dynamics in the resting state. Cereb Cortex 24:663–676.

Beckmann CF, DeLuca M, Devlin JT, Smith SM (2005): Investigations into resting-state connectivity using independent component analysis. Philos Trans R Soc B Biol Sci 360:1001–1013.

Biswal B, Yetkin FZ, Haughton VM, Hyde JS (1995): Functional connectivity in the motor cortex of resting human brain using echo-planar MRI. Magn Reson Med 34:537–541.

Bonhomme V, Boveroux P, Brichant JF, Laureys S, Boly M (2012): Neural correlates of consciousness during general anesthesia using functional magnetic resonance imaging (fMRI). Arch Ital Biol 150:155–163.

Boveroux P, Vanhaudenhuyse A, Bruno M-A, Noirhomme Q, Lauwick S, Luxen A, Degueldre C, Plenevaux A, Schnakers C, Phillips C, Brichant J-F, Bonhomme V, Maquet P, Greicius MD, Laureys S, Boly M (2010): Breakdown of within- and between-network resting state functional magnetic resonance imaging connectivity during propofol-induced loss of consciousness. Anesthesiology 113:1038–1053.

Brown EN, Lydic R, Schiff ND (2010): General anesthesia, sleep, and coma. N Engl J Med 363:2638–2650.

Brown EN, Purdon PL, van Dort CJ (2011): General anesthesia and altered states of arousal: A systems neuroscience analysis. Annu Rev Neurosci 34:601–628.

Bruce CJ, Goldberg ME, Bushnell MC, Stanton GB (1985): Primate frontal eye fields. II. Physiological and anatomical correlates of electrically evoked eye movements. J Neurophysiol 54:714–734.

Buckner RL, Vincent JL (2007): Unrest at rest: Default activity and spontaneous network correlations. NeuroImage 37:1091–1096; discussion 1097–1099.

Calhoun VD, Adali T, Pearlson GD, Pekar JJ (2001): A method for making group inferences from functional MRI data using independent component analysis. Hum Brain Mapp 14:140–151.

Chang C, Glover GH (2010): Time-frequency dynamics of resting-state brain connectivity measured with fMRI. Neuroimage 50: 81–98.

Chang C, Liu Z, Chen MC, Liu X, Duyn JH (2013): EEG correlates of time-varying BOLD functional connectivity. NeuroImage 72: 227–236.

Cole DM, Smith SM, Beckmann CF (2010): Advances and pitfalls in the analysis and interpretation of resting-state FMRI data. Front Syst Neurosci 4:8.

Cromwell TH, Eger EI 2nd, Stevens WC, Dolan WM (1971): Forane uptake, excretion, and blood solubility in man. Anesthesiology 35:401–408.

Damoiseaux JS, Rombouts SARB, Barkhof F, Scheltens P, Stam CJ, Smith SM, Beckmann CF (2006): Consistent resting-state networks across healthy subjects. Proc Natl Acad Sci USA 103: 13848–13853.

Deco G, Jirsa VK (2012): Ongoing cortical activity at rest: Criticality, multistability, and ghost attractors. J Neurosci 32:3366–3375.

Deco G, Jirsa VK, McIntosh AR (2011): Emerging concepts for the dynamical organization of resting-state activity in the brain. Nat Rev Neurosci 12:43–56.

Deco G, Jirsa V, McIntosh AR, Sporns O, Kötter R (2009): Key role of coupling, delay, and noise in resting brain fluctuations. Proc Natl Acad Sci USA 106:10302–10307.

Demirci O, Stevens MC, Andreasen NC, Michael A, Liu J, White T, Pearlson GD, Clark VP, Calhoun VD (2009): Investigation of relationships between fMRI brain networks in the spectral domain using ICA and Granger causality reveals distinct differences between schizophrenia patients and healthy controls. Neuroimage 46:419–431.

Deshpande G, Kerssens C, Sebel PS, Hu X (2010): Altered local coherence in the default mode network due to sevoflurane anesthesia. Brain Res 1318:110–121.

Detsch O, Schneider G, Kochs E, Hapfelmeier G, Werner C (2000): Increasing isoflurane concentration may cause paradoxical increases in the EEG bispectral index in surgical patients. Br J Anaesth 84:33–37.

Eger EI, II (1984): The pharmacology of isoflurane. Br J Anaesth 56 Suppl 1:71S–99S.

Engel AK, Fries P, Singer W (2001): Dynamic predictions: Oscillations and synchrony in top-down processing. Nat Rev Neurosci 2:704–716.

Flohr H (1995): An information processing theory of anaesthesia. Neuropsychologia 33:1169–1180.

Fox MD, Raichle ME (2007): Spontaneous fluctuations in brain activity observed with functional magnetic resonance imaging. Nat Rev Neurosci 8:700–711.

Franks NP (2006): Molecular targets underlying general anaesthesia. Br J Pharmacol 147 Suppl 1:S72–81.

Franks NP (2008): General anaesthesia: From molecular targets to neuronal pathways of sleep and arousal. Nat Rev Neurosci 9: 370–386.

Ghosh A, Rho Y, McIntosh AR, Kötter R, Jirsa VK (2008): Noise during rest enables the exploration of the brain's dynamic repertoire. PLoS Comput Biol 4:e1000196.

Goense JBM, Logothetis NK (2008): Neurophysiology of the BOLD fMRI signal in awake monkeys. Curr Biol 18:631–640.

Greicius MD, Kiviniemi V, Tervonen O, Vainionpää V, Alahuhta S, Reiss AL, Menon V (2008): Persistent default-mode network connectivity during light sedation. Hum Brain Mapp 29:839–847.

Handwerker DA, Roopchansingh V, Gonzalez-Castillo J, Bandettini PA (2012): Periodic changes in fMRI connectivity. NeuroImage 63:1712–1719.

Heine L, Soddu A, Gómez F, Vanhaudenhuyse A, Tshibanda L, Thonnard M, Charland-Verville V, Kirsch M, Laureys S, Demertzi A (2012): Resting state networks and consciousness: Alterations of multiple resting state network connectivity in physiological, pharmacological, and pathological consciousness States. Front Psychol 3:295.

Himberg J, Hyvärinen A, Esposito F (2004): Validating the independent components of neuroimaging time series via clustering and visualization. NeuroImage 22:1214–1222.

Hoffman WE, Edelman G (1995): Comparison of isoflurane and desflurane anesthetic depth using burst suppression of the electroencephalogram in neurosurgical patients. Anesth Analg 81:811–816.

Hudetz AG (2006): Suppressing consciousness: Mechanisms of general anesthesia. Semin Anesth Perioper Med Pain 25:196–204.

Hudetz AG (2012): General anesthesia and human brain connectivity. Brain Connect 2:291–302.

Huffman KJ, Krubitzer L (2001): Area 3a: Topographic organization and cortical connections in marmoset monkeys. Cereb Cortex 11:849–867.

Hutchison RM, Everling S (2012): Monkey in the middle: Why non-human primates are needed to bridge the gap in resting-state investigations. Front Neuroanat 6:29.

Hutchison RM, Mirsattari SM, Jones CK, Gati JS, Leung LS (2010): Functional networks in the anesthetized rat brain revealed by independent component analysis of resting-state fMRI. J Neurophysiol 103:3398–3406.

Hutchison RM, Leung LS, Mirsattari SM, Gati JS, Menon RS, Everling S (2011): Resting-state networks in the macaque at 7 T. NeuroImage 56:1546–1555.

Hutchison RM, Gallivan JP, Culham JC, Gati JS, Menon RS, Everling S (2012a): Functional connectivity of the frontal eye fields in humans and macaque monkeys investigated with resting-state fMRI. J Neurophysiol 107:2463–2474.

Hutchison RM, Womelsdorf T, Gati JS, Leung LS, Menon RS, Everling S (2012b): Resting-state connectivity identifies distinct functional networks in macaque cingulate cortex. Cereb Cortex 22:1294–1308.

Hutchison RM, Womelsdorf T, Allen EA, Bandettini PA, Calhoun VD, Corbetta M, Della Penna S, Duyn JH, Glover GH, Gonzalez-Castillo J, Handwerker DA, Keilholz S, Kiviniemi V, Leopold DA, de Pasquale F, Sporns O, Walter M, Chang C (2013a): Dynamic functional connectivity: Promise, issues, and interpretations. NeuroImage 80:360–378.

Hutchison RM, Womelsdorf T, Gati JS, Everling S, Menon RS (2013b): Resting-state networks show dynamic functional connectivity in awake humans and anesthetized macaques. Hum Brain Mapp 34:2154–2177.

Jafri MJ, Pearlson GD, Stevens M, Calhoun VD (2008): A method for functional network connectivity among spatially independent resting-state components in schizophrenia. Neuroimage 39: 1666–1681.

Jones DT, Vemuri P, Murphy MC, Gunter JL, Senjem ML, Machulda MM, Przybelski SA, Gregg BE, Kantarci K, Knopman DS, Boeve BF, Petersen RC, Jack CR, Jr (2012): Non-stationarity in the "resting brain's" modular architecture. PloS One 7:e39731.

Kalthoff D, Po C, Wiedermann D, Hoehn M (2013): Reliability and spatial specificity of rat brain sensorimotor functional connectivity networks are superior under sedation compared with general anesthesia. NMR Biomed 26:638–650.

Kannurpatti SS, Biswal BB, Kim YR, Rosen BR (2008): Spatio-temporal characteristics of low-frequency BOLD signal fluctuations in isoflurane-anesthetized rat brain. NeuroImage 40:1738–1747.

Keilholz SD, Magnuson ME, Pan W-J, Willis M, Thompson GJ (2013): Dynamic properties of functional connectivity in the rodent. Brain Connect 3:31–40.

Kiviniemi V, Jauhiainen J, Tervonen O, Pääkkö E, Oikarinen J, Vainionpää V, Rantala H, Biswal B (2000): Slow vasomotor fluctuation in fMRI of anesthetized child brain. Magn Reson Med 44:373–378.

Kiviniemi V, Vire T, Remes J, Elseoud AA, Starck T, Tervonen O, Nikkinen J (2011): A sliding time-window ICA reveals spatial variability of the default mode network in time. Brain Connect 1:339–347.

Kiviniemi VJ, Haanpää H, Kantola J-H, Jauhiainen J, Vainionpää V, Alahuhta S, Tervonen O (2005): Midazolam sedation increases fluctuation and synchrony of the resting brain BOLD signal. Magn Reson Imaging 23:531–537.

Klassen LM, Menon RS (2004): Robust automated shimming technique using arbitrary mapping acquisition parameters (RASTAMAP). Magn Reson Med 51:881–887.

Körding KP, Wolpert DM (2006): Bayesian decision theory in sensorimotor control. Trends Cogn Sci 10:319–326.

Koval MJ, Hutchison RM, Lomber SG, Everling S (2014): Effects of unilateral deactivations of dorsolateral prefrontal cortex and anterior cingulate cortex on saccadic eye movements. J Neurophysiol 111:787–803.

Leopold DA, Maier A (2012): Ongoing physiological processes in the cerebral cortex. NeuroImage 62:2190–2200.

Lewis JW, van Essen DC (2000a): Mapping of architectonic subdivisions in the macaque monkey, with emphasis on parieto-occipital cortex. J Comp Neurol 428:79–111.

Lewis JW, van Essen DC (2000b): Corticocortical connections of visual, sensorimotor, and multimodal processing areas in the parietal lobe of the macaque monkey. J Comp Neurol 428:112–137.

Li C-X, Patel S, Auerbach EJ, Zhang X (2013): Dose-dependent effect of isoflurane on regional cerebral blood flow in anesthetized macaque monkeys. Neurosci Lett 541:58–62.

Liang Z, King J, Zhang N (2011): Uncovering intrinsic connectional architecture of functional networks in awake rat brain. J Neurosci 31:3776–3783.

Liang Z, King J, Zhang N (2012): Intrinsic organization of the anesthetized brain. J Neurosci 32:10183–10191.

Liu J, Klein KW, Griffin JD, White PF (1995): Does monitoring end-tidal isoflurane concentration improve titration during general anesthesia? J Clin Anesth 7:186–191.

Liu X, Zhu X-H, Zhang Y, Chen W (2011): Neural origin of spontaneous hemodynamic fluctuations in rats under burst-suppression anesthesia condition. Cereb Cortex 21:374–384.

Liu X, Pillay S, Li R, Vizuete JA, Pechman KR, Schmainda KM, Hudetz AG (2013a): Multiphasic modification of intrinsic functional connectivity of the rat brain during increasing levels of propofol. NeuroImage 83:581–592.

Liu X, Zhu X-H, Zhang Y, Chen W (2013b): The change of functional connectivity specificity in rats under various anesthesia levels and its neural origin. Brain Topogr 26:363–377.

Logothetis NK (2002): The neural basis of the blood-oxygen-level-dependent functional magnetic resonance imaging signal. Philos Trans R Soc Lond B Biol Sci 357:1003–1037.

Logothetis NK (2008): What we can do and what we cannot do with fMRI. Nature 453:869–878.

Logothetis NK, Pauls J, Augath M, Trinath T, Oeltermann A (2001): Neurophysiological investigation of the basis of the fMRI signal. Nature 412:150–157.

Lu H, Zuo Y, Gu H, Waltz JA, Zhan W, Scholl CA, Rea W, Yang Y, Stein EA (2007): Synchronized delta oscillations correlate with the resting-state functional MRI signal. Proc Natl Acad Sci USA 104:18265–18269.

Majeed W, Magnuson M, Keilholz SD (2009): Spatiotemporal dynamics of low frequency fluctuations in BOLD fMRI of the rat. J Magn Reson Imaging 30:384–393.

Mantini D, Gerits A, Nelissen K, Durand J-B, Joly O, Simone L, Sawamura H, Wardak C, Orban GA, Buckner RL, Vanduffel W (2011): Default mode of brain function in monkeys. J Neurosci 31:12954–12962.

Mantini D, Corbetta M, Romani GL, Orban GA, Vanduffel W (2013): Evolutionarily novel functional networks in the human brain? J Neurosci 33:3259–3275.

Mars RB, Jbabdi S, Sallet J, O'Reilly JX, Croxson PL, Olivier E, Noonan MA., Bergmann C, Mitchell AS, Baxter MG, Behrens TE, Johansen-Berg H, Tomassini V, Miller KL, Rushworth MF (2011): Diffusion-weighted imaging tractography-based parcellation of the human parietal cortex and comparison with human and macaque resting-state functional connectivity. J Neurosci 31:4087–4100.

Martuzzi R, Ramani R, Qiu M, Rajeevan N, Constable RT (2010): Functional connectivity and alterations in baseline brain state in humans. NeuroImage 49:823–834.

Masamoto K, Kanno I (2012): Anesthesia and the quantitative evaluation of neurovascular coupling. J Cereb Blood Flow Metab 32:1233–1247.

Matsui T, Tamura K, Koyano KW, Takeuchi D, Adachi Y, Osada T, Miyashita Y (2011): Direct comparison of spontaneous functional connectivity and effective connectivity measured by intracortical microstimulation: An fMRI study in macaque monkeys. Cereb Cortex 21:2348–2356.

Meunier D, Lambiotte R, Bullmore ET (2010): Modular and hierarchically modular organization of brain networks. Front Neurosci 4 Available at: http://www.frontiersin.org/Neuroscience/10.3389/fnins.2010.00200/abstract. Accessed on April 28, 2011.

Mhuircheartaigh RN, Rosenorn-Lanng D, Wise R, Jbabdi S, Rogers R, Tracey I (2010): Cortical and subcortical connectivity changes during decreasing levels of consciousness in humans: A functional magnetic resonance imaging study using propofol. J Neurosci 30:9095–9102.

Moeller S, Nallasamy N, Tsao DY, Freiwald WA (2009): Functional connectivity of the macaque brain across stimulus and arousal states. J Neurosci 29:5897–5909.

Nallasamy N, Tsao DY (2011): Functional connectivity in the brain: Effects of anesthesia. Neuroscientist 17:94–106.

Nickalls RWD, Mapleson WW (2003): Age-related iso-MAC charts for isoflurane, sevoflurane and desflurane in man. Br J Anaesth 91:170–174.

Pawela CP, Biswal BB, Cho YR, Kao DS, Li R, Jones SR, Schulte ML, Matloub HS, Hudetz AG, Hyde JS (2008): Resting-state functional connectivity of the rat brain. Magn Reson Med 59: 1021–1029.

Peltier SJ, Kerssens C, Hamann SB, Sebel PS, Byas-Smith M, Hu X (2005): Functional connectivity changes with concentration of sevoflurane anesthesia. Neuroreport 16:285–288.

Pouget A, Dayan P, Zemel RS (2003): Inference and computation with population codes. Annu Rev Neurosci 26:381–410.

Qiu M, Ramani R, Swetye M, Constable RT (2008): Spatial nonuniformity of the resting CBF and BOLD responses to sevoflurane: In vivo study of normal human subjects with magnetic resonance imaging. Hum Brain Mapp 29:1390–1399.

Rabinovich MI, Friston KJ, Varona P, editors (2012): Principles of Brain Dynamics: Global State Interactions, 1st ed. Cambridge, MA, MIT Press.

Rampil IJ, Weiskopf RB, Brown JG, Eger EI, II, Johnson BH, Holmes MA, Donegan JH (1988): I653 and isoflurane produce similar dose-related changes in the electroencephalogram of pigs. Anesthesiology 69:298–302.

Rubinov M, Sporns O (2010): Complex network measures of brain connectivity: Uses and interpretations. NeuroImage 52:1059–1069.

Sadaghiani S, Hesselmann G, Friston KJ, Kleinschmidt A (2010): The relation of ongoing brain activity, evoked neural responses, and cognition. Front Syst Neurosci 4:20.

Salvador R, Suckling J, Coleman MR, Pickard JD, Menon D, Bullmore E (2005): Neurophysiological architecture of functional magnetic resonance images of human brain. Cereb Cortex 15:1332–1342.

Schrouff J, Perlbarg V, Boly M, Marrelec G, Boveroux P, Vanhaudenhuyse A, Bruno M-A, Laureys S, Phillips C, Pélégrini-Issac M, Maquet P, Benali H (2011): Brain functional integration decreases during propofol-induced loss of consciousness. NeuroImage 57:198–205.

Shmuel A, Leopold DA (2008): Neuronal correlates of spontaneous fluctuations in fMRI signals in monkey visual cortex: Implications for functional connectivity at rest. Hum Brain Mapp 29:751–761.

Shmuel A, Augath M, Oeltermann A, Logothetis NK (2006): Negative functional MRI response correlates with decreases in neuronal activity in monkey visual area V1. Nat Neurosci 9:569–577.

Smith SM, Fox PT, Miller KL, Glahn DC, Fox PM, Mackay CE, Filippini N, Watkins KE, Toro R, Laird AR, Beckmann CF (2009): Correspondence of the brain's functional architecture during activation and rest. Proc Natl Acad Sci USA 106:13040–13045.

Swank RL, Watson CW (1949): Effects of barbiturates and ether on spontaneous electrical activity of dog brain. J Neurophysiol 12:137–160.

Tagliazucchi E, von Wegner F, Morzelewski A, Brodbeck V, Laufs H (2012): Dynamic BOLD functional connectivity in humans and its electrophysiological correlates. Front Hum Neurosci 6:339.

Teichert T, Grinband J, Hirsch J, Ferrera VP (2010): Effects of heartbeat and respiration on macaque fMRI: Implications for functional connectivity. Neuropsychologia 48:1886–1894.

Tinker JH, Sharbrough FW, Michenfelder JD (1977): Anterior shift of the dominant EEG rhytham during anesthesia in the Java monkey: Correlation with anesthetic potency. Anesthesiology 46:252–259.

Tononi G (2004): An information integration theory of consciousness. BMC Neurosci 5:42.

van Essen DC (2004): Surface-based approaches to spatial localization and registration in primate cerebral cortex. NeuroImage 23 Suppl 1:S97–107.

van Essen DC, Drury HA, Dickson J, Harwell J, Hanlon D, Anderson CH (2001): An integrated software suite for surface-based analyses of cerebral cortex. J Am Med Inform Assoc 8: 443–459.

van Meer MPA, van der Marel K, Otte WM, Berkelbach van der Sprenkel JW, Dijkhuizen RM (2010): Correspondence between altered functional and structural connectivity in the contralesional sensorimotor cortex after unilateral stroke in rats: A combined resting-state functional MRI and manganese-enhanced MRI study. J Cereb Blood Flow Metab 30:1707–1711.

Vincent JL, Patel GH, Fox MD, Snyder AZ, Baker JT, van Essen DC, Zempel JM, Snyder LH, Corbetta M, Raichle ME (2007): Intrinsic functional architecture in the anaesthetized monkey brain. Nature 447:83–86.

von der Malsburg C, Phillips WA, Singer W editors (2010): Dynamic Coordination in the Brain: From Neurons to Mind. Cambridge, MA, MIT Press.

Wang K, van Meer MPA, van der Marel K, van der Toorn A, Xu L, Liu Y, Viergever MA, Jiang T, Dijkhuizen RM (2011): Temporal scaling properties and spatial synchronization of spontaneous blood oxygenation level-dependent (BOLD) signal fluctuations in rat sensorimotor network at different levels of isoflurane anesthesia. NMR Biomed 24:61–67.

White NS, Alkire MT (2003): Impaired thalamocortical connectivity in humans during general-anesthetic-induced unconsciousness. NeuroImage 19:402–411.

Zhao F, Zhao T, Zhou L, Wu Q, Hu X (2008): BOLD study of stimulation-induced neural activity and resting-state connectivity in medetomidine-sedated rat. NeuroImage 39:248–260.